Geological Quarterly, 2025, 69, 40
DOI: https://doi.org/10.7306/gq.1813

Modelling earthquake and palaeotsunami damage scenarios on the eastern Mediterranean coast between ~300–551 CE: implications for the archaeological site of Porphyreon on the Phoenician coast of Lebanon

Radosław STANISZEWSKI[1, *], Anna WYSOCKA[2], Anna FILIPEK[2], Urszula WICENCIAK[3], Anna Maria KOTARBA-MORLEY[4] and Tomasz WALISZEWSKI[5]

[1] University of Warsaw, Faculty of Geology, Żwirki i Wigury 93, 02-089 Warszawa, Poland; ORCID-0009-0005-3517-2317

[2] Polish Academy of Sciences, Institute of Geological Sciences, Twarda 51/55, 00-818 Warszawa, Poland; ORCID: 0000-0003-1015-5033 [A.W.], 0000-0003-2861-4058 [A.F.]

[3] Polish Centre of Mediterranean Archaeology, University of Warsaw, Tyniecka 15/17, 02-630 Warszawa, Poland; ORCID-0000-0001-6475-5523

[4] University of Adelaide, School of Humanities, Faculty of Arts, Business, Law and Economics, XHFF+P2 Bedford Park, Adelaide, Australia; ORCID-0000-0002-0069-3834

[5] University of Warsaw, Faculty of Archaeology, Krakowskie Przedmieście 26/28, 00-927 Warszawa, Poland; ORCID-0000-0002-5793-4600

Staniszewski, R., Wysocka, A., Filipek, A., Wicenciak, U., Kotarba-Morley, A.M., Waliszewski, T., 2025. Modelling earthquake and palaeotsunami damage scenarios on the eastern Mediterranean coast between ~300–551 CE: implications for the archaeological site of Porphyreon on the Phoenician coast of Lebanon. Geological Quarterly, 69, 40; https://doi.org/10.7306/gq.1813

The eastern Mediterranean has long been shaped by the impacts of natural disasters, notably tsunamis and earthquakes, with several major events recorded during the Late Roman and Byzantine periods (specifically between 300–551 CE). This study focuses on the ancient anchorage at Porphyreon on the Phoenician coast and integrates results from numerical earthquake modelling with contextual geological and archaeological field studies. Here, we explore the high potential of correlating diverse records to discern specific signatures of past earthquake and tsunami events. Our study modelled 42 fault zones located in the eastern Mediterranean to identify those capable of generating earthquakes strong enough to cause tsunami-driven flooding and destruction at Porphyreon. Of the 42 scenarios analysed, twelve magnitude 7 earthquakes could have potentially impacted the southern coast of Cyprus and the south-eastern Mediterranean coast in the Late Roman and Byzantine periods. Our analyses identify a fault system that could have posed a major threat to the Phoenician coast during the 551 CE earthquake, with calculated maximum tsunami wave heights exceeding 2.6 m. Our secondary outcome is the identification of faults that remain capable of generating tsunami waves today, posing a continuing threat to the coasts of Lebanon and Cyprus and their occupants.

Key words: palaeotsunami; tsunami modelling; ~300-551 CE earthquakes; Porphyreon/Phoenicia; Archaeology of Lebanon; Late Roman and Byzantine periods.

INTRODUCTION

The eastern Mediterranean region has experienced numerous catastrophic earthquakes and tsunamis throughout its geological and historical past, significantly impacting coastal settlements and shaping human history. Coastal areas are routinely inundated by storm, cyclone and, less frequently, tsunami waves, events which have operated throughout geological history, albeit occasionally at catastrophic scales. While many studies document such phenomena primarily in shoreface and offshore facies sequences (cf. Shanmugam, 2006; Shiki et al., 2021), the intensive development of coastal settlements since the onset of the Holocene has significantly increased the vulnerability of human populations to these marine hazards (cf. Scheffers and Kelletat, 2003; Shanmugam, 2012). In this study, we integrate numerical tsunami modelling with contextual archaeological and geological data to investigate whether an extreme marine event, which occurred sometime between ~300–551 CE, may have affected the coastal zone at Porphyreon (modern-day Jiyeh; Fig. 1) an ancient anchorage site situated on the Phoenician coast of Lebanon.

Multidisciplinary palaeotsunami research has become increasingly critical to both geology and archaeology in recent decades, offering insights into past coastal dynamics, disaster impacts on ancient civilisations, and informing present-day hazard assessments. The catastrophic tsunami that struck Suma-

* Corresponding author, e-mail: r.staniszewski@uw.edu.pl

Received: June 23, 2025; accepted: September 29, 2025; first published online: November 14, 2025

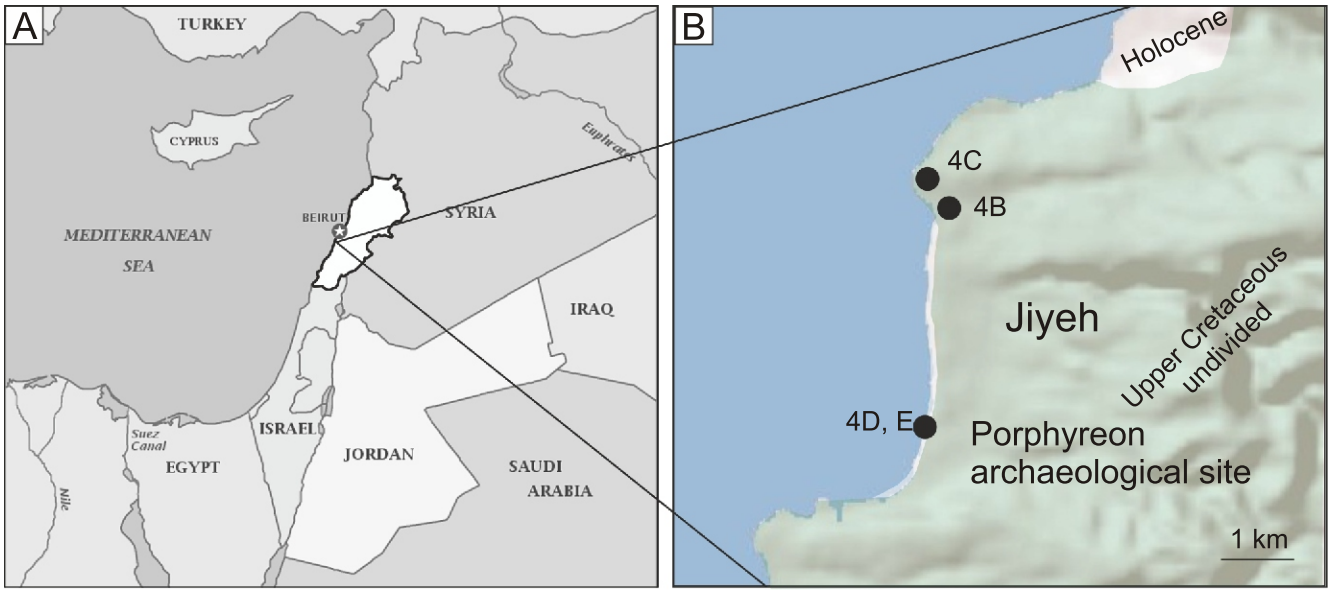

Fig. 1A – political map of the eastern Mediterranean, Lebanon area – in white, highlighted by outline (modified from https://www.yourchildlearns.com/online-atlas/lebanon-map.htm), study area – enlarged on part B of the figure; B – simplified geology around the Porphyreon archaeological site (after Zumoffen, 1926) and study points location, black dots mark the locations of photos in Figure 4

tra and the Indian Ocean rim on 26 December 2004 significantly heightened awareness and intensified research efforts into tsunami hazards, extending attention to the Mediterranean, and especially the Eastern Mediterranean (host to major centres of ancient civilisations), and its coastal communities. Many studies into tsunami hazards have emerged from this area, notably from coastal regions of Lebanon (Sbeinati et al., 2005), the Aegean coastlines (Papadopoulos et al., 2014; Altinok et al., 2011), Israel (Salamon et al., 2010), southern Turkey (Bruins et al., 2008), and the broader Levantine coastline (Marriner and Pirazzoli, 2006).

Recent events, including the earthquake and tsunami that struck Samos on 30 October 2020, and the devastating earthquake affecting the Turkish-Syrian border region on 6 February 2023, have further reinforced our understanding of the vulnerability of this region – often referred to as the "cradle of civilisation" – to seismic activity. Consequently, the question of identifying evidence for past undersea earthquakes and their tsunamis, which may have had catastrophic consequences for ancient coastal settlements, has become increasingly critical. Against this backdrop, the ancient anchorage site of Porphyreon, with its archaeological record spanning historical periods from the Iron Age all the way through to the Roman and Byzantine periods, and its coastal location and vulnerability, presents a valuable opportunity to test and refine methods that integrate historical sources, numerical tsunami modelling, and limited archaeological and geological field data. By exploring these interconnections, our study aims to contribute not only to understanding the site's complex occupation history but also to broader regional assessments of tsunami hazards and their historical consequences.

The past two decades have been rich in historical (e.g., Stiros, 2001; Meier, 2007), geoarchaeological (e.g., Goodman-Tchernov et al., 2009; Fischer et al., 2016; Goodman-Tchernov, 2020; Salamon et al., 2024) and seismological studies (e.g., Ambraseys, 2009; Ambraseys and Synolakis, 2010), each of which, usually within their own discipline, attempted to organise our knowledge of this area. The abundance of these research initiatives led to the emergence of a kind of neo-catastrophism in the study of the Mediterranean Basin past (Ambraseys, 2005; Morhange and Marriner, 2010; Morhange et al., 2014; Liritzis et al., 2019; cf. also Vött et al., 2019). However, recent interdisciplinary work conducted at Mediterranean ports and coastal passage sites such as Caesarea Maritima, Tel Ashqelon, and the Messina Strait clearly demonstrated that integrating historical, geoarchaeological, and seismological datasets offer the opportunity for a more nuanced and reliable reconstruction of the timing, dynamics, and impacts of Late Antique tsunami events (Reinhardt et al., 2006; Dey and Goodman-Tchernov, 2010; Dey et al., 2014; Barbano et al., 2014; Hoffman et al., 2018; Salamon et al., 2024).

Numerical modelling has become a widely used methodological tool in geological research, including for understanding fault-zone mechanics (e.g., Donzé et al., 1994; Zhang and Sanderson, 1996; Wang et al., 2008; Konon et al., 2016; Romano et al., 2017), earthquake dynamics (e.g., Mikumo and Miyatake, 1983; Ismail-Zadeh and Soloviev, 2022), and tsunami wave propagation (e.g., Heinrich et al., 2001; Dutykh et al., 2011; Sugawara, 2021; Tadibaght et al., 2022; Salamon et al., 2024). Despite the growing number of studies employing numerical tsunami modelling, relatively few integrate these methods with classical sedimentological approaches (Falvard and Paris, 2017; Nigg et al., 2021), and fewer still explicitly combine digital modelling with analyses of sedimentological processes and archaeological records (cf. Sbeinati et al., 2005; Sánchez-Sánchez et al., 2022). To bridge this gap, this study integrates numerical modelling of historical tsunami events that impacted the eastern Mediterranean Sea with limited sedimentological observations and contextual archaeological evidence. Specifically, our objective is to assess, through numerical modelling, whether historically documented earthquakes in the region could have generated tsunami waves capable of depositing high-energy gravel layers identified at the Porphyreon archaeological site.

Our modelling approach incorporates data from 135 earthquake scenarios across 42 faults in the southeastern Mediterranean, including seven onshore and 34 offshore structures (Figs. 2 and 3). Given the limited nature of available field data,

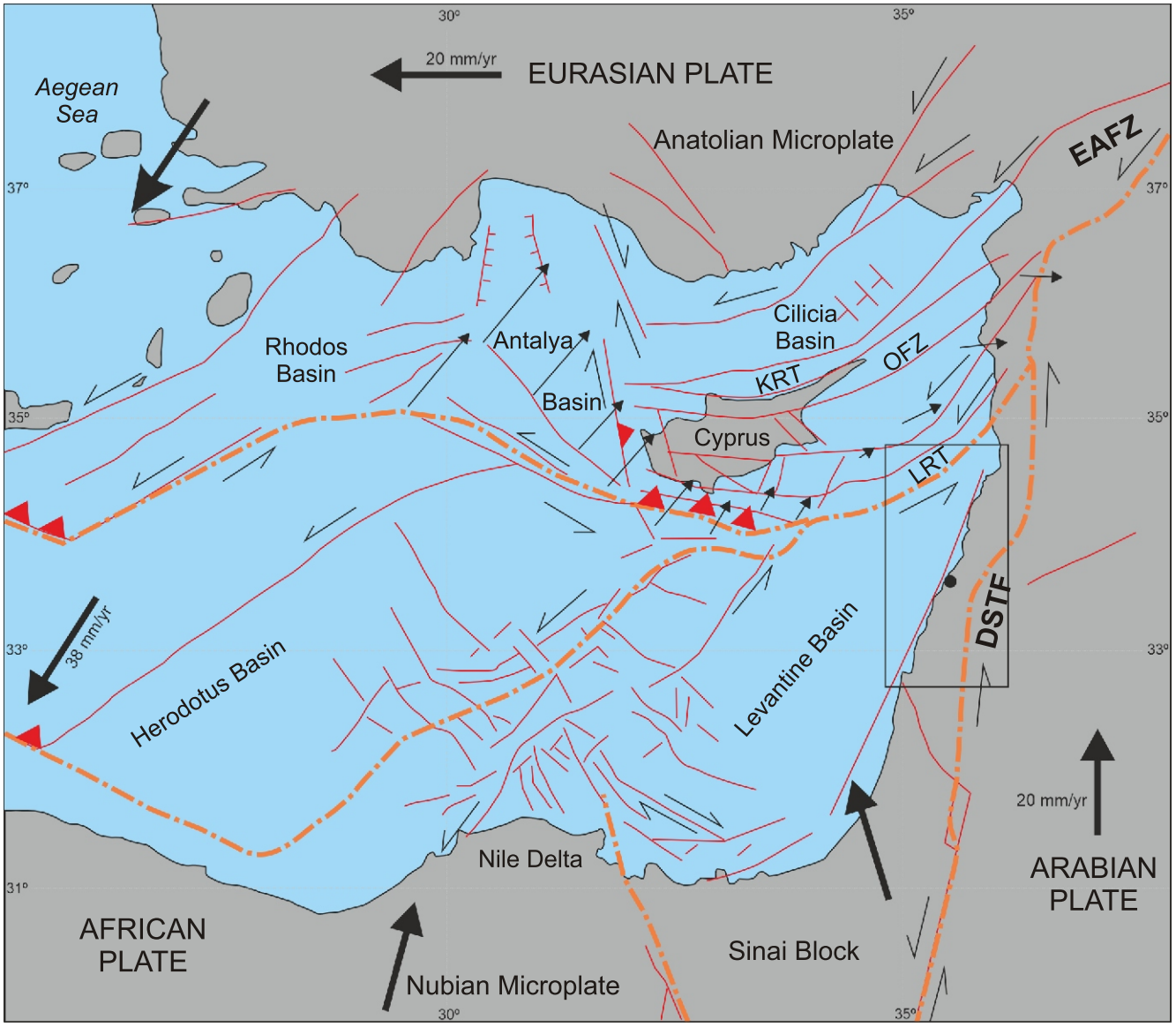

Fig. 2. Major tectonic features of the Eastern Mediterranean, adopted from Harrison et al. (2013)

DSTF – Dead Sea transform fault, EAFZ – Eastern Anatolian fault zone, LRT – Larnaca Ridge transform fault, OFZ – Ovgos fault zone, KRT – Kyrenia Range thrust system. Explanations: bold orange dashed lines – major crustal boundaries, red lines – regional faults, large arrows – relative plate motion, half arrows – relative horizontal motion along faults, thin full arrows – relative motion between the Anatolian microplate and African plate, black dot – study area, box – the area for which the maximum tsunami height was modelled (see Fig. 12)

including the absence of absolute dates for the gravel deposits, we rely primarily on relative dating provided by archaeological stratigraphy: the gravel layer overlies a Late Roman occupation surface (4th–6th century CE) and is sealed by later construction material. Within this temporal framework, we evaluate the likelihood that several historically documented earthquakes coincide with the formation of the deposit. Although our aim is not to definitively attribute the gravel layer to any single historical event, this study demonstrates how integrating incomplete archaeological records with numerical tsunami modelling can significantly narrow down plausible scenarios, especially in regions where sites access can often be limited, and field data remain fragmentary or inaccessible.

Historical research, particularly analyses of ancient textual sources and the terminology employed for describing natural disasters (such as earthquakes and tsunamis) in Late Antiquity (e.g., the use of terms such as *seismos*, *kataklysmos* or *tremor* in hagiographies and chronicles), allows identification of periods in which the Lebanese coast may have experienced such catastrophic events, further informing the plausibility of the hypothesised event scenario (e.g., Antonopoulos, 1987; Guidoboni et al., 1994; Fokaefs and Papadopoulos, 2007; Dey and Goodman-Tchernov, 2010; Salamon et al., 2010; Altinok et al., 2011; Papadopoulos et al., 2012, 2014; Maramai et al., 2014). Ancient Latin and Greek written sources describe the interval between ~300 and 551 CE as particularly marked by devastating earthquakes and tsunamis, each of which significantly impacted settlements on the coasts of Syria, Phoenicia or Palestine. These include the significant events of 2 April 303 CE (Sidon; Ambraseys, 2009), 341/342 CE (Salamis in Cyprus; Guidoboni et al., 1994), 347/348 CE, 21 July 365 CE (Crete; Papadopoulos et al., 2012), 9 July 551 CE (Berytus/Beirut; Mordechai, 2020), and, finally, 18 January 749 CE (Caesarea Maritima; Salamon et al., 2010). Contemporary authors of hagi-

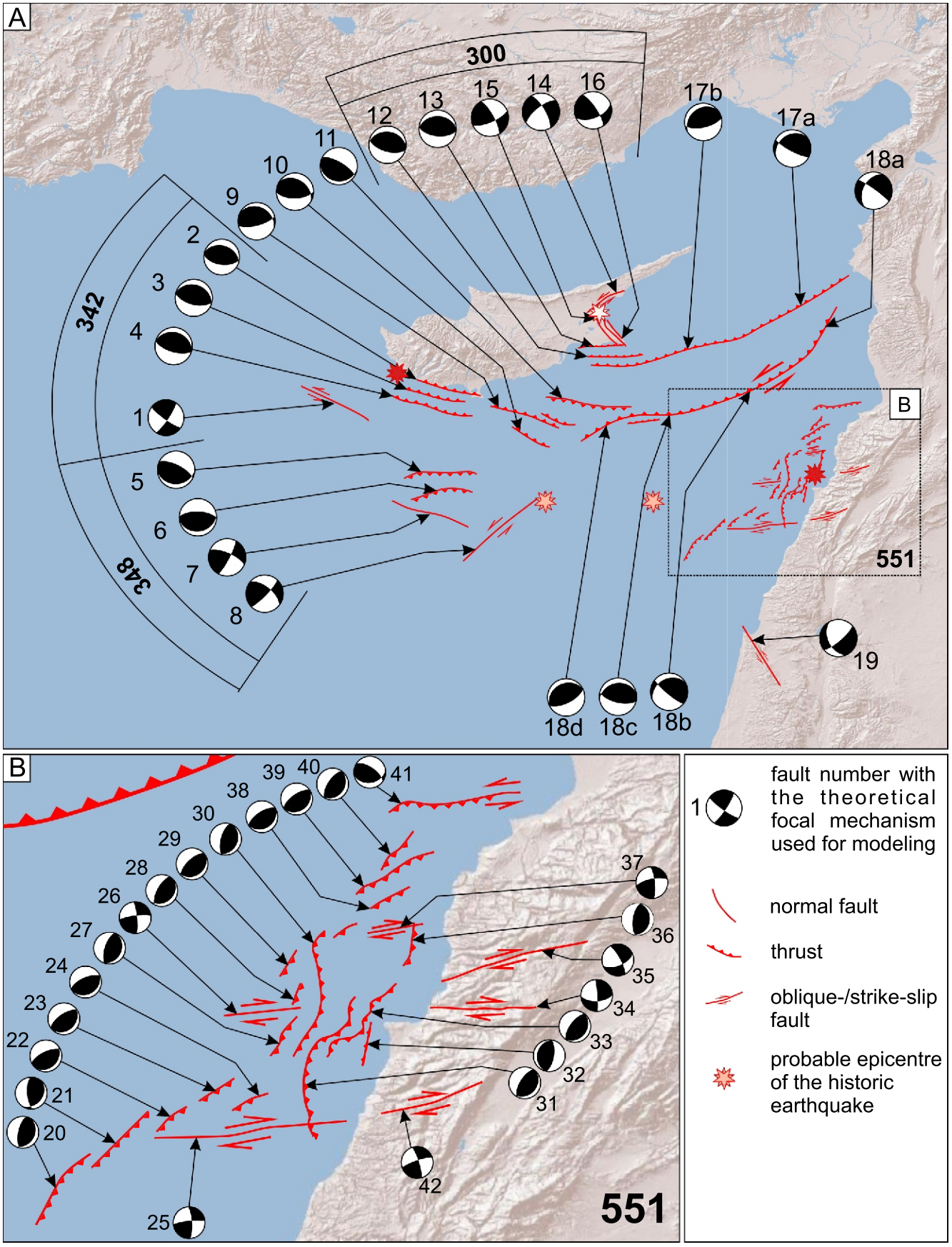

Fig. 3A – location of faults and theoretical focal mechanisms used for modelling; B – enlarged box from Figure 3A to show strike-slip faults associated with the Mount Lebanon and Tripoli-Beirut thrusts associated with the 551 CE earthquake

Location of historical epicentres based on Altinok et al. (2011). Focal mechanism based on the USGS Earthquake Catalogue database

ographies and chronicles – such as Jerome, Sozomen, Agathias Scholasticus, John of Ephesus and John Malalas – often provided very detailed accounts of the devastating effects of earthquakes and their ensuing tsunamis (Papadopoulos, 2021). Specifically, historical sources record a major submarine earthquake on 9 July 551 CE, with its epicentre likely located between Cyprus and the Levantine coast, which devastated numerous towns including Berytus (Beirut), and was possibly accompanied by tsunami waves (Mordechai, 2020; Papadopoulos, 2021). Ambraseys (2009), in his comprehensive review, provided detailed assessments regarding their chronology, possible tsunami waves and their possible extent (also see Guidoboni et al., 1994; Maramai et al., 2014).

The Porphyreon archaeological site (Fig. 1), located directly on the Mediterranean Sea shore, originated as a settlement in the Late Bronze Age, with reoccupation during the Iron Age following a break in habitation (hiatus), and continued through the Persian period (13th–5th centuries BCE). It later developed into a town during the Hellenistic, Roman, and Late Antique periods (4th/3rd century BCE to 7th century CE), and became known in later historical sources as Jiyeh or Nebi Younis. Our archaeological investigations conducted between 2003 and 2014 provided evidence of a settlement in the vicinity of Jiyeh (Lebanon, south of Beirut; Papadopoulos, 2021; Fig. 1), dating back to at least the 9th to 8th centuries BCE, which appears to have flourished until the mid-7th century CE – in line with the evidence relating to Porphyreon.

During rescue excavations carried out in the summer of 2005, a cultural deposit with an approximately 35 cm-thick, contiguous gravel layer was discovered and documented in an open section along the beach, directly adjacent to the Porphyreon archaeological site (Wicenciak and El-Tayeb, 2006; Figs. 1 and 4). Due to time constraints and local political factors at play, we were unable to further interpret this phenomenon, and no sediment samples were collected during that season. When site was revisited in 2021, the exposure was found to have been completely destroyed (Fig. 4D, E). Renewed excavations were not possible owing to the unstable political and security situation in the region, and further work was suspended for safety reasons. As a result, it was not possible to conduct detailed sedimentological characterisation, to examine the composition of individual sediment layers, or to determine whether there are marine fossils or reworked archaeological materials (such as recycled pottery fragments) within them. In view of the absence of direct field data, the 2005 photographic documentation was re-analysed in order to properly interpret the origin of the layer with pebbles and to identify sedimentological structures indicative of high-energy depositional processes. As a result, a working hypothesis was formulated proposing a tsunami-origin of the gravel layer. In order to critically evaluate this hypothesis, additional research methods were applied. We decided to undertake numerical modelling based on open-source data accessible from the USGS Earthquake Catalogue, supplemented by available geological and archaeological data.

Given the nature of our limited field dataset, the aim of our study has always been not to directly confirm the tsunami origin of the gravel layer. Rather, our goal was to test a methodological approach that integrates incomplete archival evidence with numerical modelling to assess whether tsunami scenarios generated by known historical earthquakes could plausibly account for the observed stratigraphy. We believe that this approach may also prove applicable to other archaeological sites where only fragmentary or incomplete evidence exists, particularly in regions that are currently inaccessible to researchers due to political instability, armed conflict, rapid urban development, or the destruction of sites by natural disasters. In such cases, where field documentation is limited, outdated, or relies heavily on archival records collected decades earlier, the integration of numerical modelling with existing archaeological and geological data, supplemented by analyses of historical sources, can offer a valuable framework for generating and testing hypotheses. We hope that by using our example and applying this methodological model, researchers may gain greater confidence to revisit fragmentary datasets, re-examine archival materials, and propose new interpretations for sites that would otherwise remain poorly understood or overlooked.

GEOLOGICAL SETTING

Our research area for tsunami modelling covers the eastern part of the Mediterranean Sea (Figs. 1 and 2), with a specific focus on the coast of Lebanon and the archaeological site of Porphyreon at Jiyeh (Waliszewski and Gwiazda, 2015; Wicenciak, 2016; Fig. 1). The site occupies much of the southern part of a shallow bay formed by rocky spurs. In the immediate vicinity, limestones and coarse-grained sandstones of Cretaceous and Neogene age are exposed (Fig. 4A–C; Nader, 2014), despite the presence of Quaternary deposits (Fig. 4D). As a result, the coastline around Jiyeh is geologically quite diverse. Several distinct shoreline types can be distinguished here: (i) natural, vertical exposed rocky cliffs or headlands; (ii) flat, coarser-grained or gently sloping exposed abrasive platforms shaped by waves action or low, exposed rocky beaches with larger boulders, (iii) coarse-grained sandy beaches, moderately sloping or with a steeper slope, (iiii) beaches composed of a mix of sand, gravel, pebbles and/or shells.

The Mediterranean Sea, situated between present-day shifting lithospheric plates, is one of the most seismically active regions on Earth. It is bounded by the Eurasian, Arabian and African plates, and dissected by a complex network of transform and normal faults, and thrusts (e.g., Harrison et al., 2013; Aksu et al., 2021; Faysal et al., 2023; Fig. 2). One of the significant tectonic features in this area is the Dead Sea Transform Fault (Fig. 2), which extends northwards as the Jordan Valley Fault and splays into several strike-slip faults, including the Râchaiya, Serghaya, Yammouneh and Roűm faults (Erdik et al., 2014; Fig. 5). In addition, significant thrust faults, some of which extend offshore, are located west of Mount Lebanon, including the Mount Lebanon and Tripoli-Beirut thrusts (Fig. 5). This geological complexity results in significant seismic activity over modern, historical and geological timescales (Guidoboni et al., 1994; Morhange et al., 2006; Maramai et al., 2014; Nemer et al., 2023). Over the past 30 years alone, the study area has recorded more than 2,300 earthquakes with a magnitude greater than 2.5 (USGS Earthquake Catalogue, 2021 – https://earthquake.usgs.gov/). From the 17th century BCE to 1999, 44 tsunami events have been documented across the Mediterranean Basin, with the oldest known record dating back to 426 BCE (Antonopoulos, 1987; Guidoboni et al., 1994; Sbeinati et al., 2005; Fokaefs and Papadopoulos, 2007; Maramai et al., 2014; Papadopoulos et al., 2014).

HISTORICAL EVIDENCES OF TSUNAMIS IN THE STUDY AREA

In historical sources, tsunamis are rarely described in terms that allow for an unambiguous identification of their triggering mechanism. Where possible, however, it is important to distinguish between tsunamis generated by seismic activity (earth-

Fig. 4A – general view of the northern part of the Jiyeh; note the rocky coast and exposures of solid rocks on the upper part of the shore. For the close-ups of points indicated by arrows – see (B) (C); B – exposure of the white pelitic limestones; C – grey stratified bioclastic sandstones; D – sandy, wide flat part of the coast in Jiyeh (as of 2021), white box – escarpment along the beach; E – sequence of sandy and gravelly beds clearly visible in the cliff along the beach; the 2005 archive photo of the area of the white box from photo D. The length of the vertical scale is 30 cm

quakes) and those that may be related to submarine landslides or other triggering factors. This distinction is crucial for assessing the likelihood of a tsunami occurrence at specific locations and periods, and it underpins the following analyses of individual events. Between ~300 and 551 CE, over 100 earthquakes and associated phenomena are recorded in historical sources, of which approximately a dozen are reported to have produced secondary effects such as tsunamis (Guidoboni et al., 1994; Ambraseys, 2009; Maramai et al., 2014). However, caution is required, as some events analysed by Ambraseys (2009), Guidoboni et al. (1994), or Maramai et al. (2014) appear to be somewhat questionable or problematic; ancient authors occasionally confused or conflated facts by combining separate multiple earthquakes into single incidents, as in the case of 368 CE

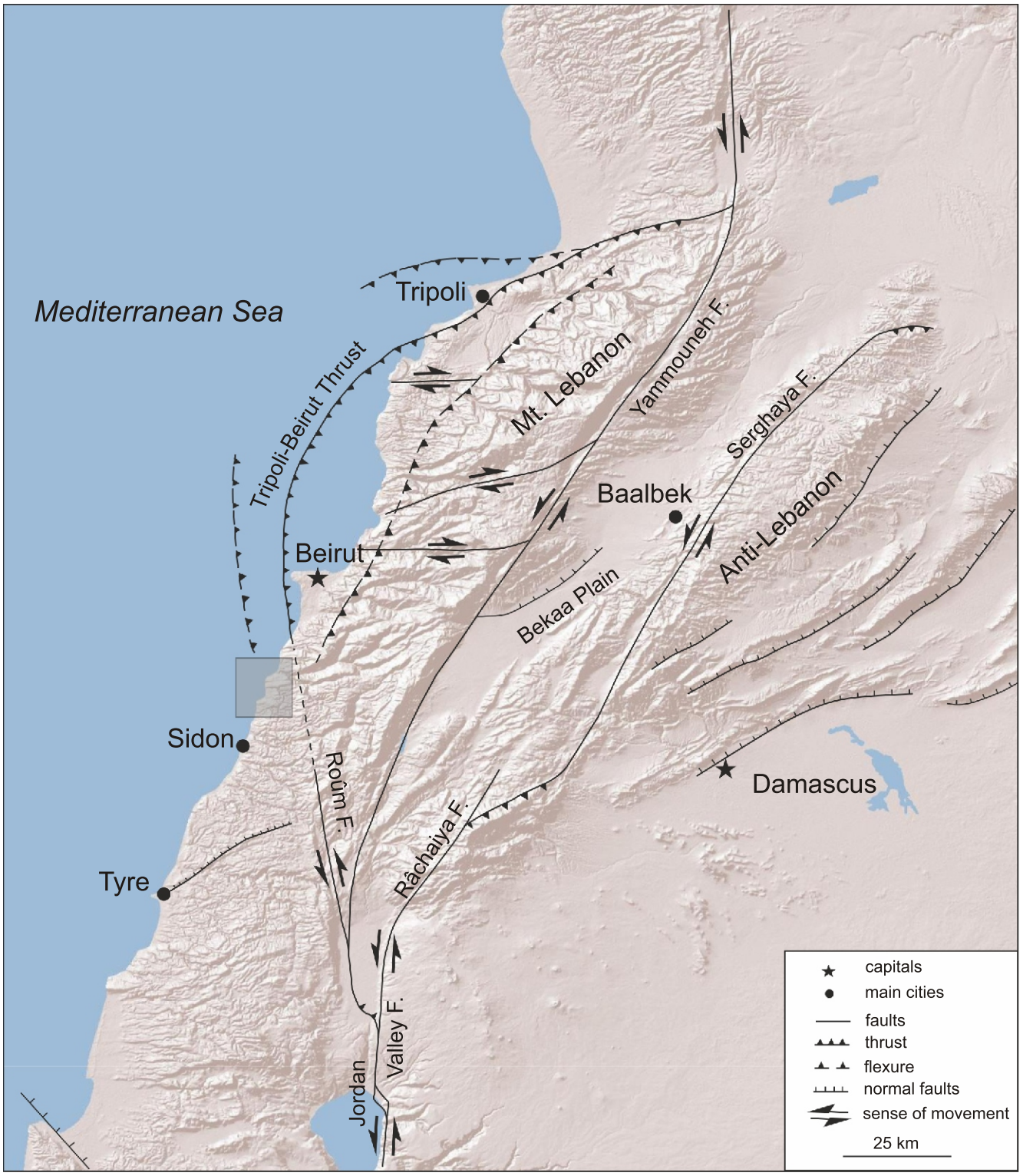

Fig. 5. Map of the active faults in Lebanon and neighbouring areas (on the ESRI Shaded Relief background; fault interpretation after Erdik et al., 2014)

Small grey box – see Figure 1B

in Nicaea (cf. Ambraseys, 2009). Many of these recorded events were highly localised, affecting only a single settlement and its close vicinity, such as in the case of Antioch on the Orontes or Constantinople (e.g., 303 CE – Eusebius (MPal); Ambraseys, 2009; 341/342 CE – Guidoboni et al., 1994; 347/348 CE – Ambraseys, 2009; 365 CE – Papadopoulos et al., 2012; Salamon et al., 2010; 455 CE – Ambraseys, 2009; 502 CE – Trombley, 2000; 551 CE – Darawcheh, et al., 2000; Sbeinati et al., 2005; Hall, 2004; Ambraseys, 2009). The predominance of the major urban centres in the record of earthquakes is also a result of their greater recognition among contemporary and later authors, reflecting their sphere of interest and extent of their knowledge.

Furthermore, many of these earthquakes occurred inland, away from the coastal areas (such as the Palestine and Arabia earthquakes in 363 CE or 418 CE), and thus had no direct impact on the Phoenician coast at the time, which is the primary focus of this study. Without independent verification by other means, such as through further, refined geological or archaeological analyses (cf. Reinhardt et al., 2006; Dey and Goodman-Tchernov, 2010; Ward, 2016), it remains difficult to corroborate historical accounts of the extent and nature of the destruction suffered by these localities. By way of example, the correlation of geomorphological studies with data from archaeological and historical sources, such as those undertaken at the harbours of Sidon and Tyre, offer compelling evidence for correlating the Late Antique semi-abandonment phases of the harbours to tsunamigenic events (Marriner et al., 2006, 2008).

However, over the ~250-years period considered in this study (~300–551 CE), several events are recorded that may have reached and impacted on the coast of present-day Lebanon. Between 293 and 306 CE, an earthquake was recorded at Salamis in Cyprus, resulting in a tsunami wave. A significant and well-documented event is recorded in ancient chronicles, occurring on 2 April 303 CE, when extensive destruction affected the cities of Sidon, Tyre, and possibly Byblos farther north. The tsunami wave generated by this earthquake is said to have reached Caesarea Maritima, where it reportedly cast ashore the body of the martyr Apphian, as recorded by Eusebius of Caesarea (Eusebius MPal 325/1478, cf. Bardy, 1958). Other minor earthquakes, of which little is known about their extent or tsunamigenic potential, are mentioned in 331–332 CE and again in 341/342 CE at Salamis in Cyprus, and in 347 CE or 348 CE at Beirut.

A major widespread tsunamigenic event occurred on 21 July 365 CE, initiated by a powerful earthquake off Crete, which then spread, generating a large tsunami wave that subsequently impacted the coasts of Egypt and the Peloponnese. In September 455 CE, another earthquake was recorded near Tripolis in Phoenicia, reportedly causing damage across much of today's Lebanese coastline. On 22 August 502 CE, another event of catastrophic proportions was recorded around Akko at the southern end of the Phoenician coast. Sources from the period speak of the destruction of half of Tyre and Sidon although, according to some accounts, only the synagogue in Beirut (Berytus) was destroyed (Trombley, 2000).

What became truly memorable for generations of Syrians, Phoenicians and Palestinians was the great earthquake and resulting tsunami of 9 July 551 CE. Its epicentre was probably located under the seabed between present-day Lebanon and Cyprus, with the city of Beirut suffering the greatest devastation. The events at Berytus were reported by several contemporaneous authors, including John Malalas (2000; Chronographia 485), Ps. Dionysius of Tel Mahre (Chronicle 134–135 in Witakowski, 1996) and Agathias (Histories 2.15.2-3), all living in the 6th century CE and writing about events occurring during their lifetime (sources compiled in Darawcheh, 2000; Sbeinati et al., 2005; cf. also Hall, 2004; Ambraseys, 2009). Based on written accounts, the course of events suggests two tremors separated by several hours, with a tsunami reported to have occurred in the interval between them. During this time, the sea is said to have retreated 1–2 Roman miles (~1,480–2,960 metres) exposing shipwrecks and sunken cargo, which coastal residents rushed to salvage, before the returning wave claimed many lives. The resulting destruction extended along the entire Phoenician coast, from Tyre in the south to Tripolis and perhaps as far north as Arados. Major destruction was recorded at the cities of Tyre, Sidon, Berytus, Byblos, Tripolis, and at the Ras Chekka promontory, where a large section of the rocky cape collapsed into the sea, creating a new harbour. The greatest devastation, however, was suffered by Berytus, where a huge fire following the second shock and collapse of buildings led to the deaths of up to 30,000 people (Ant. Plac. 159, cf. Geyer, 1965). If references to the temporary relocation of the renowned law school from Berytus to Sidon are accurate (Agathias II.15, cf. Frendo, 1975), it suggests that the areas south of Beirut (Berytus) must have suffered comparatively less destruction.

Notably, the "tidal" wave described in historical sources appears to correlate with the effects of a tsunami generated by a submarine earthquake and/or by submarine landslides (Salamon et al., 2010, 2024). It is particularly noteworthy that these events were reported to have occurred in Berytus, just 28 km north of Porphyreon (Jiyeh), which is the focus of our attention due to the evidence under analysis.

The events cited above indicate a period of intensified seismic activity compared with other historical periods documented in the eastern Mediterranean (cf. Ambraseys, 2009). However, only a limited number of these events resulted in destructive tsunami waves that directly threatened the Phoenician coastline, including the region between Berytus and Sidon, where the site of Porphyreon is located. Among these, two events stand out: that of 2 April 303 CE and the particularly destructive earthquake of 9 July 551 CE, both of which had a significant regional impact, especially along the Phoenician coast. By contrast, the tsunami of 21 July 365 CE affected a much wider area of the Mediterranean, including parts of Egypt, Libya, Greece and the Levant (Salamon et al., 2010; Papadopoulos et al., 2012). Other potentially relevant seismic events include those recorded in in 341/342 CE near Salamis in Cyprus, and in 347/348 CE at Berytus. Although no direct archaeological or geological evidence of the 365 CE tsunami has yet been identified along the southern or central coast of ancient Phoenicia, several studies have documented tsunami-related deposits attributed to this event in neighbouring regions, including Israel, Cyprus and Egypt (Goodman-Tchernov et al., 2009; Reicherter et al., 2009; Salamon et al., 2010).

METHODS AND MATERIALS

The research methods employed in this study encompass (i) numerical modelling, (ii) sedimentological interpretation of archive materials, (iii) analyses of available archaeological stratigraphic evidence, and iv) historical and textual source review, integrated into a multidisciplinary framework. The archaeological data were derived from the archaeological excavations conducted in 2005 (Wicenciak and El-Tayeb, 2006; Waliszewski and Gwiazda, 2015; Wicenciak, 2016) and re-assessed through later stratigraphic and ceramic analyses. Historical earthquake records and terminologies used in ancient textural evidence were critically examined to aid chronological correlation and scenario validation.

Numerical modelling. Numerical modelling was a key methodological tool in this study, aimed at simulating tsunami wave propagation generated by historical earthquakes in the eastern Mediterranean. The study area, from which faults were selected, extends between the coasts of Cyprus and Lebanon (Figs. 2 and 3). The selection of specific epicentres and their corresponding historical earthquake events was guided by archaeological data associated with Porphyreon and other coastal sites in Lebanon. The time interval for our analysis was refined using historical data, ceramic typology and stratigraphic dating, as detailed in later sections. In addition, comprehensive desk-based analyses incorporated geological (Zumoffen, 1926; Nader, 2014; Nader et al., 2018) and structural evidence (Salah-Eldin and El-Khoury, 2004; Hawie et al., 2013; Kinnaird and Robertson, 2013; Fernández-Blanco et al., 2020), tectonic maps (Lemenkova, 2021), and seismic profiles (Carton et al., 2009; Bowman, 2011; Skiple et al., 2012; Hawie et al., 2013, 2017) to identify potential fault zones capable of generating tsunamis in the study area and to support fault selection and scenario construction.

Based on epicentres documented in the literature (summarised by Brax et al., 2019), the faults were categorised into four groups, each associated with specific historical earthquake events:

1. South-east coast of Cyprus in c. 300 CE (Guidoboni et al., 1994; Fokaefs and Papadopoulos, 2007; Ambraseys, 2009).
2. South-west coast of Cyprus in 342 CE (Ambraseys, 1962; Soysal et al., 1981; Soysal, 1985; Antonopoulos, 1987; Guidoboni et al., 1994; Soloviev et al., 2000; Ambraseys, 2009).
3. Eratosthenes Seamount region in 348 CE (Soysal et al., 1981; Guidoboni et al., 1994; Yolsal et al., 2007; Ambraseys, 2009).
4. Beirut (ancient Berytus) region in 551 CE (Soysal et al., 1981; Guidoboni et al., 1994; Darawcheh et al., 2000; Sbeinati et al., 2005; Fokaefs and Papadopoulos, 2007; Ambraseys, 2009).

Numerical modelling techniques formed a key component of this study and were employed to simulate the propagation of tsunami waves based on data from contemporary seismic stations. The main controlling factors influencing the generation of earthquakes – and, indirectly, tsunamis – were considered to be fault geometry (length, width, strike, dip, depth, depth to top) and dislocation parameters (strike, rake, slip, shear modulus). Subsequently, these were utilised in the course of further analyses. We analysed the earthquakes with epicentres located in the south-eastern Mediterranean taking into the account the geological structure of the region. To facilitate tsunami wave propagation modelling, we used the *MIRONE* software package (for details see Luis, 2007) which incorporates TINTOL code (http://fct-gmt.ualg.pt/mirone/downloads/windows.html, accessed December 2022) for hydrodynamic processes simulation. The method used in this study follows that of Omira et al. (2009), in which the initial disturbance on the sea surface – caused by seafloor deformation – is calculated using algorithms developed by Mansinha and Smylie (1971). All simulations were scenario-based and are summarised in Figure 6.

The subsequent step involved modelling the deformation of the seafloor surface using the EMODnet Digital Bathymetry (DTM 2020) and the models proposed by Mansinha and Smylie (1971). This approach was selected based on its computational efficiency and its ability to minimise the uncertainties commonly associated with input parameters. To further reduce sensitivity to poorly constrained variables the model was configured to calculate exclusively the vertical component of earthquake-induced deformation. For the tsunami propagation simulation, a time step of 1.5 seconds was used, and calculations were performed for a duration of 3,000 seconds from the wave excitation. To accomplish this, we considered several key parameters, including hypocentre depth, fault angle, dip and displacement slip, and shear modulus, all of which were based on present-day seismological datasets. Where direct information was unavailable, values were inferred from geological cross-sections and regional seismic profiles. In the absence of detailed fault geometry data, we made the following assumptions: 80° for slip faults, 25° for thrust faults, and 60° for normal faults. Hypocentre depths for the model were obtained from the USGS Earthquake Catalogue database, provided the relevant fault had exhibited seismic activity within the observational timeframe of the seismic stations. Where no direct information was available, the hypocentre was assumed to be located at the midpoint of the total fault depth. Fault dip and direction of displacement were determined using focal mechanism interpolations data available through the USGS Earthquake Catalogue. In instances where this information was lacking, the direction of displacement was estimated by drawing analogies from other tectonically similar regions worldwide. The slip parameter was defined as the minimum displacement required to achieve a specific earthquake magnitude.

In this study, we focused on modelling earthquakes of magnitude 7 and above (7.5 and 8) due to their greater likelihood of generating tsunami waves with destructive potential. Although lower-magnitude events (e.g., M6.5–6.9) have occasionally produced tsunamis, these are typically highly localised and rarely result in significant inundation along the eastern Mediterranean coast. Moreover, our modelling parameters prioritised scenarios with wave heights exceeding one metre, consistent with thresholds documented in historical tsunamigenic events in this region (cf. Salamon et al., 2010; England et al., 2015). The decision to exclude sub-M7 scenarios is therefore based on both historical precedent and the expected energy release required to match the sedimentary signatures observed at Porphyreon. In addition, several faults within the study region were physically too short to generate earthquakes of such magnitudes (7 or higher), further justifying this methodological threshold.

To assess the feasibility of earthquake occurrence along each fault, we applied an empirical relationship criterion established by Scholz (1982). Earthquake magnitude was calculated using a formula proposed by Aki (1966):

$$M_0 = \mu \underline{u} S$$

where: M_0 – represents the seismic moment of the component couple of the equivalent double couple, μ – the rigidity modulus, $\underline{u}$ – denotes the average amount of dislocation (slip), S – the area of the fault surface area.

For a rectangular fault, the surface area (S) can be calculated as the product of its length (L) and width (W) (S = LxW). Three different shear modulus variants were assigned, depending on the depth and lithology of the hypocenter. For faults occurring within the sedimentary cover, a shear modulus of 2.6 was adopted. For faults located at greater depths, a value of 4.4 was used, while a shear modulus of 6.8 was applied to faults situated above 25 km depth (Geist and Bilek, 2001). Thickness estimates for the sedimentary cover were obtained from the sedimentary cover map published by Aksu et al. (2021).

Sedimentological interpretation of the archive materials. Given the absence of direct sedimentological field studies – due to destruction of the exposed section and further issues of access to the site – the interpretation of the sedimentary processes at Porphyreoon was necessarily based on secondary

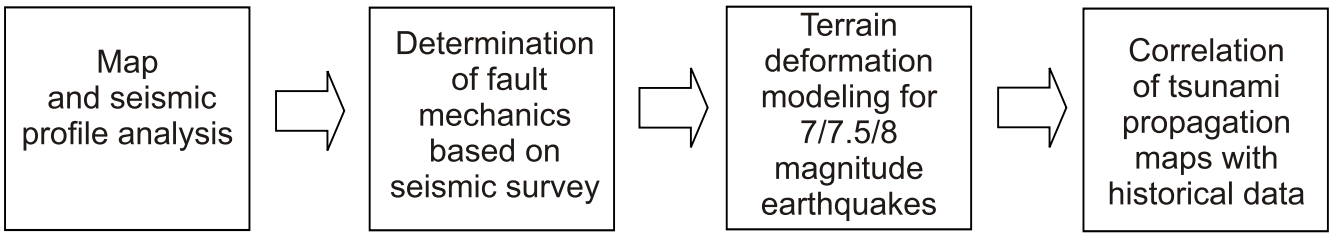

Fig. 6. A flowchart for the numerical modelling of earthquake and related tsunami scenarios

documentation. Our primary dataset comprised detailed photographic archive and field drawings from 2005 rescue excavations, supplemented by published literature, geological mapping, and contextual information drawn from site reports and from other excavations we conducted at the site between 2003 and 2014. As no sediment cores, samples, or stratigraphic columns were preserved, this interpretive component remains constrained by the quality and completeness of visual documentation and must therefore be considered inferential in nature.

The sedimentary unit of interest – a distinctive, laterally extensive gravel deposit – was therefore assessed for its grain size distribution, internal organisation, and sedimentary structures as observable in the photographic record. Indicators such as poor sorting, imbrication, abrupt basal contacts, and vertical grading were identified and used to propose high-energy depositional mechanisms. However, due to the limitations of the dataset, it was not possible to carry out the grain-size analysis, mineralogical characterisation or microfossil identification that are typically used to distinguish tsunami from storm or fluvial deposits – another possibility we refer to below. As a result, the sedimentological findings presented here are interpreted as supplementary to the scenario-based tsunami modelling, rather than as standalone evidence.

To mitigate these interpretive limitations, the sedimentological assessment was contextualised using independent lines of evidence. Archaeological stratigraphy, derived from the excavation reports (Wicenciak and El-Tayeb, 2006; Waliszewski and Gwiazda, 2015; Wicenciak, 2016), provided temporal bracketing for the gravel unit, which was identified within an occupation sequence dated between the 4th and 6th centuries CE. This chronology was supported by diagnostic ceramic typologies found above and below the deposit, allowing correlation with known seismic events in the historical record. The absence of cultural artefacts within the gravel lens and its stratigraphic separation from architectural features further suggested a non-anthropogenic origin.

Historical texts describing regional earthquakes and marine disturbances – such as those of 303 CE, 348 CE, and 551 CE – were also consulted to establish plausible deposition windows. These sources provided critical information about coastal damage, inundation, and seismicity, enhancing the contextual interpretation of the gravel layer as a potential tsunami deposit. Nonetheless, as acknowledged in our Discussion, alternative depositional processes such as storm surge or rapid erosion linked to extreme rainfall events cannot be definitively ruled out given the current dataset.

Accordingly, the sedimentological interpretation presented here should be understood as exploratory and contingent. It complements the more robust evidence provided by the numerical tsunami modelling and archaeological stratigraphy but is limited by the indirect nature of the data. Future research involving targeted coring, sediment sampling, and laboratory analyses will be essential for confirming or revising the interpretations proposed in this study.

RESULTS

NUMERICAL SIMULATION OF THE TSUNAMI WAVE PROPAGATION

Numerical simulation serves as an effective approach for estimating the areas susceptible to inundation, as well as to determine the maximum wave height and tsunami propagation over time. Based on the simulations conducted, maximum water height maps were generated to illustrate the propagation of tsunami waves in the area near the shore (Fig. 7). Simulations for an earthquake with a magnitude of 7, 7.5 and 8 (later described as M7, M7.5 and M8) were performed for selected faults (Table 1). Among these simulations, only a subset generated tsunami waves that propagated towards the Lebanese coast (Fig. 7 and Table 1). The specific simulations that generated waves off the Lebanese coast were 8, 9, 17, 17a, 17b, 18, 18c, 20, 21, 25, 30, 31, 33, 39, and 41 (Table 1). The faults labelled as thrust faults were 9, 17, 17a, 17b, 18, 18a, 18b, 18c, 20, 21, 30, 31, 39, and 41, with a dip direction roughly perpendicular to the Lebanese coastline. Scenarios 8 and 25 represented oblique-slip faults (Fig. 4). In terms of slip measurements, the largest offset was modelled for fault 8, with a slip of 14 metres, corresponding to a M8 earthquake. Conversely, the smallest offset was observed in scenario 17, modelling a tsunami caused by a M7 earthquake, where the fault slip measured 0.2 metres (see Appendix 1 for details).

Table 1

List of faults (numbering according to Fig. 3) for which magnitude 7, 7.5 and 8 earthquakes were simulated

	Earthquake magnitude		
	7	7.5	8
Faults* capable of generating a given earthquake magnitude	1, 2, 3, 4, 5, 6, 7, 8, 9, 10, 11, 12, 13, 14, 15, 17, 17a, 17b, 18, 18a, 18b, 18c, 19, 20, 21, 25, 26, 30, 31, 33, 34, 35, 39, 41, 42	1, 2, 3, 4, 5, 6, 7, 8, 9, 11, 17, 17a, 17b, 18, 18a, 18b, 18c, 19, 25, 30, 31, 35	2, 7, 8, 17, 17b, 18
Faults* capable of generating a given earthquake magnitude and tsunami wave propagating towards the Lebanese coast	8, 9, 17, 17a, 17b, 18, 18c, 20, 21, 25, 30, 31, 33, 39, 41	8, 9, 17, 17a, 17b, 18, 18c, 25, 30, 31	8, 17, 17b, 18

* – fault locations see Figure 3

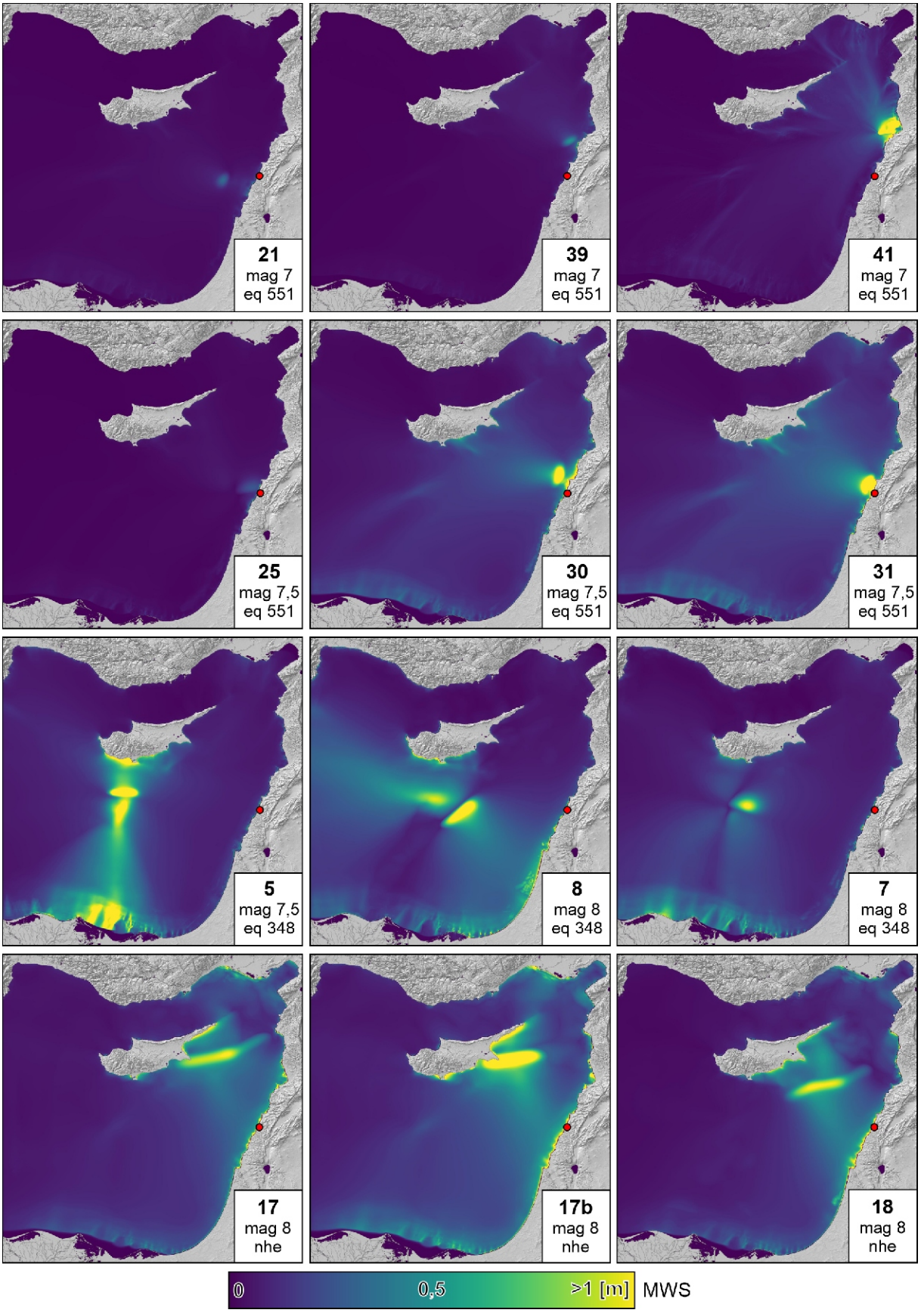

Fig. 7. Tsunami wave propagation maps for selected scenarios (data for all scenarios – see Appendix 1) expressed as maximum wave height

Red dot – study area; MWS – maximum water surface; nhe – never happened earthquake

Table 2

Summary of faults on which historical earthquakes of magnitude 7 have occurred and the maximum height of tsunami waves (in metres) along the eastern Mediterranean coast

Earthquake	Fault	Cites on the eastern coast of Mediteranean Sea													Magnitude
		Haifa	Tyre S	Tyre N	Sarepta	Sidon	**Porphyreon**	Beirut S	Beirut N	Halat	Kfaraabida	Chekka	Miniyeh	Tartus	
342 CE	1	0.2	0.2	0.2	0.1	0.1	0.1	0	0.1	0.1	0.1	0	0.1	0.1	7.5
	2	0.2	0.2	0.2	0.1	0.1	0.1	0	0.1	0.1	0.1	0	0.1	0.1	8.0
	3	0.2	0.2	0.2	0.1	0.3	0.1	0.1	0.1	0.1	0.1	0.1	0.1	0.1	7.5
	4	0.2	0.3	0.3	0.1	0.5	0.1	0.1	0.1	0.1	0.2	0.1	0.1	0.1	7.5
348 CE	5	0.3	0.5	0.7	0.3	0.9	0.5	0.2	0.3	0.8	0.3	0.3	0.2	0.2	7.5
	6	0.1	0.3	0.2	0.1	0.4	0.2	0.1	0.2	0.2	0.1	0.1	0.1	0.1	7.5
	7	0.2	1	0.8	0.5	1.3	0.4	0.2	0.4	0.7	0.3	0.2	0.3	0.2	8.0
	8	0.6	1.5	1.7	0.5	1.8	0.5	0.3	0.3	0.4	0.3	0.3	0.3	0.2	8.0
	9	0.4	1.1	1.1	0.6	1.6	0.8	0.5	0.5	1.1	0.3	0.8	0.3	0.4	7.5
	10	0	0.1	0.1	0	0.2	0.1	0	0	0.1	0	0	0	0	7.0
	11	0.4	0.4	0.3	0.2	0.5	0.2	0.2	0.1	0.7	0.3	0.4	0.3	0.3	7.5
300 CE	12	0.1	0.2	0.1	0.1	0.2	0.1	0.1	0.1	0.1	0.1	0.1	0.1	0.1	7.0
	13	0.1	0.2	0.1	0.1	0.2	0.1	0	0	0.1	0.1	0.1	0.1	0	7.0
	14	0	0	0	0	0	0	0	0	0	0	0	0	0	7.0
	15	0	0	0	0	0.1	0	0	0	0	0	0	0	0	7.0
	16	0	0.1	0.1	0	0.1	0.1	0	0.1	0.1	0.1	0	0.1	0	7.0
	17a	0.2	0.5	0.4	0.2	0.4	0.2	0.1	0.2	0.2	0.2	0.2	0.2	0.2	8.0
	17b	1.1	1.7	2.4	1.2	2.2	1.2	0.7	0.9	0.9	0.5	0.6	1	0.7	8.0
	17	0.7	1.2	1.9	0.9	1.8	1	0.7	1	0.9	0.6	0.9	1.1	0.6	8.0
	18a	0.2	0.4	0.3	0.2	0.5	0.1	0.1	0.2	0.2	0.1	0.2	0.3	0.1	7.5
	18b	0.1	0.4	0.4	0.2	0.9	0.2	0.2	0.3	0.4	0.3	0.2	0.1	0.2	7.5
	18c	0.2	0.5	0.8	0.4	1.3	0.4	0.2	0.3	0.7	0.2	0.2	0.2	0.3	7.5
	18	0.8	1.6	2.1	1	2.2	1.1	0.6	0.8	0.9	0.4	0.4	0.5	0.6	8.0
	19	0.4	0.3	0.2	0.1	0.2	0.1	0	0	0.1	0	0	0.1	0	7.5
551 CE	20	0.1	0.4	0.4	0.2	0.5	0.2	0.1	0.1	0.2	0.1	0.1	0.1	0	7.0
	21	0.1	0.3	0.4	0.4	0.7	0.3	0.1	0.1	0.3	0.1	0.1	0.1	0.1	7.0
	25	0.1	0.4	0.4	0.4	1.1	0.3	0.2	0.1	0.3	0.2	0.1	0.1	0.1	7.5
	26	0	0.1	0.1	0	0.1	0.1	0	0.1	0.1	0.1	0.1	0	0	7.0
	30	0.4	0.8	0.9	0.5	2.4	1.3	1.4	1.3	3.2	0.7	0.7	0.5	0.3	7.5
	31	0.4	1.1	1.1	0.6	2.8	2.6	1.4	0.7	1.3	0.5	0.5	0.5	0.3	8.0
	33	0	0.2	0.1	0.1	0.3	0.1	0.1	0.1	0.2	0.1	0	0.1	0	7.0
	34	0	0	0	0	0.1	0	0.1	0.1	0.1	0	0	0	0	7.0
	35	0	0.1	0	0	0.1	0	0.1	0.1	0.1	0.1	0.1	0	0	7.5
	39	0.1	0.3	0.2	0.1	0.4	0.2	0.1	0.3	0.8	0.9	0.8	0.2	0.2	7.0
	41	0.1	0.1	0.1	0.1	0.3	0.2	0.2	0.2	0.5	0.2	1.4	1.2	0.4	7.0
	42	0	0	0	0	0.1	0	0	0	0	0	0	0	0	7.0

Shades of green indicate waves that do not reach a height of 0.5 m, yellow and orange – waves that do not exceed 3 m, red shades – tsunami waves with the greatest height, higher than 3 m

The tsunami waves that reached the Lebanese coast in many instances were characterised by relatively low heights, indicating limited potential for significant damage on land. In particular, the effects resulting from M7 earthquakes were generally discrete. Among the scenarios calculated for different faults, the strongest impact at the coast was observed for faults 10 (0.2 m); 12–16 (0.2 m), 20 (0.5 m), 21 (0.7 m), 26 (0.1 m), 33 (0.3 m), 34 (0.1 m), 39 (0.9 m), 41 (1.4 m) and 42 (0.1 m), with the corresponding maximum wave heights reported (refer to Table 2). For M7.5 earthquakes, fault scenarios resulted in maximum wave heights ranging from 0.5 m to 2 m. Notably, faults 4 (0.5 m), 5 (0.9 m), 9 (1.6 m), 11 (0.7 m), 18a (0.5 m), 18b (0.9 m), 18c (1.3 m), 25 (1.1 m), and fault 30 (reaching an astonishing 3.2 m) generated waves of varying heights (refer to Table 2). In the case of M8 earthquakes, fault 7 generated waves with a height of 1.3 m, fault 8 (1.8 m), 17b (2.4 m), 17 (1.9 m), 18 (2.2 m), while fault 31 generated waves with a maximum height of 2.8 m (Table 2). The calculated maximum tsunami wave height for the Porphyreon area is 2.6 m (scenario 31).

When considering historical earthquakes, it is evident that specific faults still pose potential threats to the Lebanese coast. For the 342 CE earthquake, it was the case only for fault 4, located southwest of the Cyprus coast (Fig. 3A), while for the 348 CE earthquake, the greatest threat was associated with fault 8 (Figs. 3A and 7), which is an oblique-slip fault situated in the central part of the Levantine Basin that generates waves that propagate directly towards the Lebanese coast (Fig. 7). For the 551 CE earthquake, most faults contributed to a potential threat, but the highest level of concern is assigned to faults 30, 31, 39, and 41 (Figs. 3B and 7), all of which are associated with the Mount Lebanon and Tripoli-Beirut Thrusts. This finding aligns well with Elias et al. (2007) and Salamon et al. (2024), who suggested that the 551 CE earthquakes, attributed to the active thrusting of Mount Lebanon, followed by a tsunami, resulted in the destruction of numerous coastal cities of Phoenicia (modern-day Lebanon, cf. Mordechai, 2020).

SEDIMENTOLOGICAL INTERPRETATIONS

The archaeological site of Porphyreon is situated in the vicinity of a beach, within an extensive, low-lying coastal region (Fig. 1). The nearest hard bedrock exposures outcrops can be found ~1 km south and 2 km north of the site (Fig. 4A–C). A distinct morphological boundary occurs on the landward side, positioned ~3 km east of the exposure. Thus, the Jiyeh area exhibits the characteristics of a small bay, with a low-lying expanse that may be susceptible to flooding during intense storms, particularly in the event of a tsunami.

During the archaeological rescue excavations along the modern shoreline, a layer of white gravel was observed and documented within the cultural strata (Wicenciak and El-Tayeb, 2006; Waliszewski and Gwiazda, 2015; Wicenciak, 2016; Figs. 8 and 9). The exposed profile, ~84 m long, captured a section of the slope eroded by storm waves and construction activities (Fig. 8). Above and below this layer, ceramic-bearing strata containing fragments of pottery and other archaeological artifacts were identified. For clarity, Arabic numerals (e.g., layer 6, 7) refer to archaeological stratigraphy, while Roman numerals (I–VII) denote sedimentological subdivisions within the gravel deposit as illustrated in Figure 10. The layers described below (labelled II–VI) correspond to the internal sedimentary subdivisions in the gravel layer (layer 6), as interpreted from the photographic and field documentation collected in 2005 (Wicenciak and El-Tayeb, 2006). These layers were identified based on various textural and structural features and are illustrated in Figure 10.

The gravel layer exhibits distinct internal stratification, as shown in Figure 10B. Just above the ceramic-bearing layer 2b (marked as I in sedimentary succession – Fig. 10B), a distinct erosional surface can be observed, accompanied by an erosional lag composed of large oval, angular to medium-rounded cobbles of white rocks, with a maximum diameter of up to 10 cm (II). Positioned above this is a layer of coarse-grained sands with poor sorting, mixed with small rock debris and highly crushed artifacts (III). This sand layer gradually transitions into a gravel layer (IV). Layer IV is composed of flat, blade- and disc-shaped white pebbles, aligned with their longer axes parallel (see Fig. 10A). Such pebble shapes are characteristic of sedimentation found in 'pebble beaches' (e.g., Krumbein, 1941; Williams and Caldwell, 1988; Hill, 2022). These pebbles likely originated from the Cretaceous rock exposures located to the north or south of the study area (Fig. 4A–C) and were likely deposited on the shore by unusually high-energy waves.

Moreover, this layer demonstrates a distinct bipartition, the lower part (IV') exhibiting reverse grading, while the upper part (IV") displays normal grading. Layers V and VI are situated above this division. Both layers are characterised by poor sorting and a massive structure. In layer V, small pebbles are randomly embedded within the sandy matrix. Layer VI, similar to layer III, consists of coarse-grained sand of very poor sorting and an admixture of small rock debris and highly crushed artifacts. Layer VII represents the upper ceramic-bearing layer 7. The transitions between the various subdivisions (II–VI) are commonly indistinct and transient. The possibility that the deposit represents a deliberately arranged construction layer was considered but ultimately dismissed. Such an interpretation is undermined by the absence of associated architectural elements, or evidence of ground preparation, or levelling fillings under the deposit which are a common occurrence on archaeological sites in the region. In addition, the irregular spatial distribution and extent and internal structure of the deposits (including gradation and lack of compaction) are inconsistent with anthropogenic formation processes and instead suggest deposition by natural high-energy events.

These features strongly indicated that the sedimentary sequence examined (II–VI from Fig. 10B) was formed in a single depositional event of varying intensity, potentially associated with the propagation of tsunami or powerful storm waves onto the coastal region. Significantly, no well-rounded pebbles with spherical shapes were discovered in the stratigraphic section observed, effectively excluding the possibility of gravel material being transported through a fluvial environment, where periodic watercourses flow from the east towards the coast.

ARCHAEOLOGICAL INTERPRETATION

Archaeological investigations conducted between 2003 and 2014 provided evidence of a settlement at the site dating back to at least the 9th to 8th centuries BCE. This settlement, and later the town of Porphyreon, thrived until the mid-7th century CE, serving as a local centre of trade and production. While the archaeological excavations at Porphyreon revealed a multiphase occupation sequence spanning from the Iron Age to the Late Antique period, particular attention in this study is directed towards a laterally extensive (visible along 32 m of an open section), 35 cm-thick, gravel deposit (Fig. 9A, B) whose atypical characteristics warranted further interpretation, albeit within the constraints of limited post-excavation documentation and the absence of in situ sedimentological sampling. Although it seems that part of the gravel layer was reused in ancient times as a functional surface, several factors argue against its anthropogenic origin. The deposit extends discontinuously

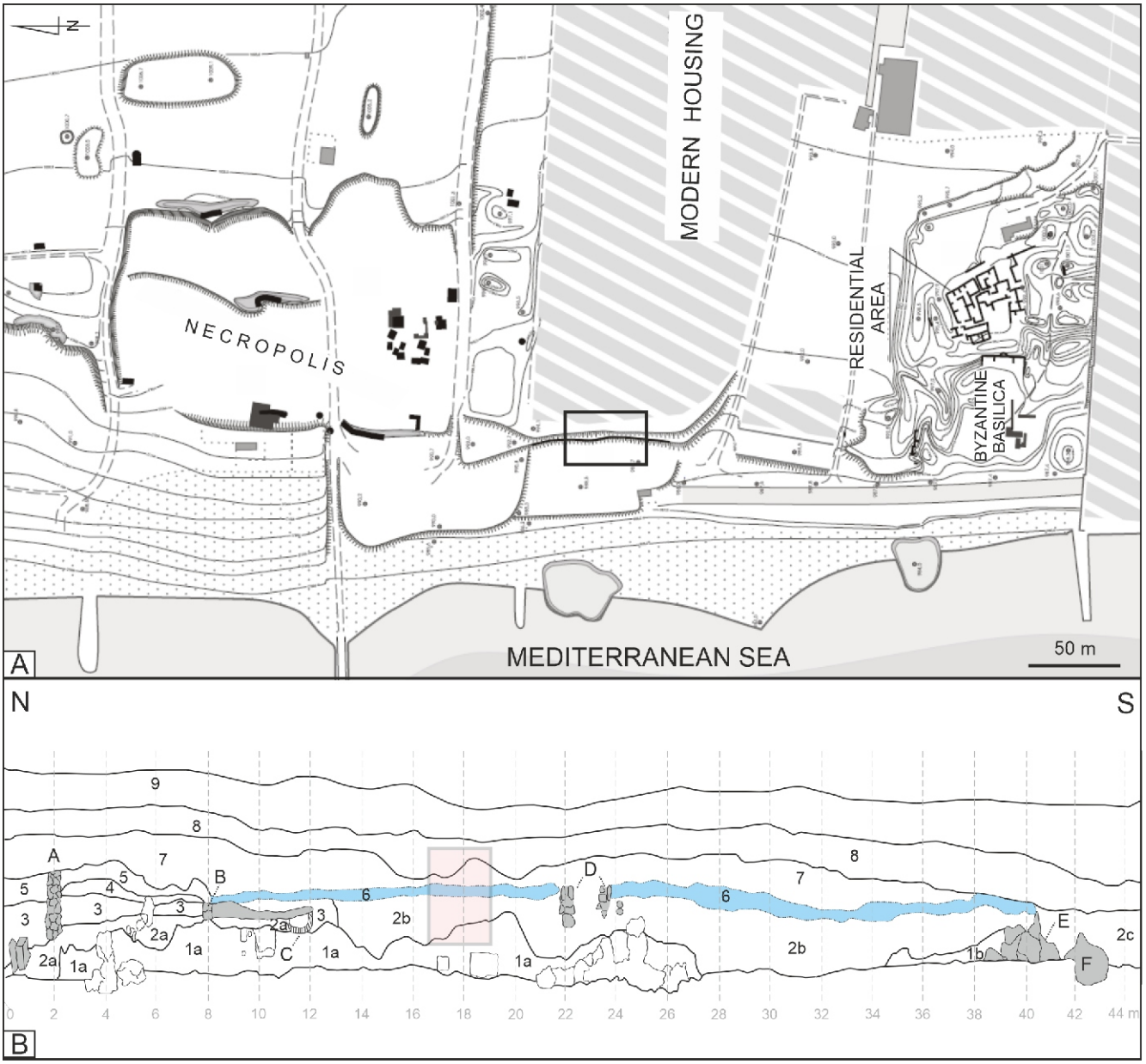

Fig. 8A – plan of the archaeological Porphyreon site in Jiyeh; box – escarpment along the beach with the part of the site where in 2005 the profile was exposed (drawn by M. Puszkarski, Polish Centre of Mediterranean Archaeology, University of Warsaw); B – sketch of a cross-section, part of the profile studied (location – box on Fig. 8A), 1a – 9 – numbers of identified archaeological layers (for details see Table 3), A–F – identified fragments of building remnants (see Table 4). To enhance the visibility of the gravel layer, the vertical scale of Figure 8B has been exaggerated

along a profile and consists of well-sorted, naturally rounded pebbles, with internal stratification (including reverse and normal grading) inconsistent with deliberate construction. Furthermore, no associated architectural features, subsoil layers or preparation surfaces have been identified below it, supporting our interpretation of a natural high-energy depositional event rather than a man-made installation.

The gravel layer was visible in a section (between 2003–2014), situated directly along the seashore (Fig. 8A), between the archaeological site (containing residential buildings and a Byzantine Basilica) ~100 m away, and the pottery production zone and the necropolis to the north of the area (Wicenciak and El Tayeb, 2006). The profile was oriented on a north-south axis, with the surveyed section being 54 m long (of which 44 m are shown on Fig. 8B). Similar to the ancient residential section, this sector formed part of a tell, an artificial hill that accumulated successive layers of natural and anthropogenic origin due to modern agricultural activity and craft activities in antiquity. The exposed stratigraphic profile was created contemporaneously, as a result of construction works to widen the area adjacent to the beach and was documented during rescue excavation research conducted by our team during the period of 2003–2014. At its highest point, the profile reached a height of over 4 m (northern section), while at its lowest point it is ~1.5–0.5 m (southern section). Five layers (9, 8, 7, 2 and 1/cf. Table 3) extend along almost its entire length (Fig. 8B).

Table 3

List and description of layers 1a–9 in Figure 8B

Layer	Description	Non-ceramic material	Pottery Dating AM/CW/TFW	Layer dating
9	humus	–	–	modern
8	dune	–	–	modern
7	compact layer of light brown earth with fragments of pottery	plaster, ashes	TFW: 3rd to mid 7th c. CE AM: mid-5th c. CE – 7th c. CE (M334) CW: -	Early Byzantine
6	natural layer; 13-15 metre of section used as floor (mortar layer was applied over pebbles)	–	–	
5	very compact dark brown and gray earth with a lot of small fragments of pottery	pottery wasters	TFW: 5th–6th c. CE AM: mid-5th c. CE – 7th c.CE (M334) CW: –	Early Byzantine
4	a layer of brown earth with many pottery sherds	small fragments of glass, bones	–	?
3	a layer of brown earth with many medium-sized stones	–	TFW: 3rd–5th c. CE AM: ER CW: ER	Mix: Early Roman to Early Byzantine
2a	a layer of brown/grey earth with many stones and sherds	–	TFW: mid 2nd c. BCE to Augustan AM: Hellenistic (CSA)/ca. 125 BCE CW: mid 2nd to mid 1st c. BCE; 1st–2nd c. CE	Late Hellenistic to Early Roman
2b	a layer of brown/grey earth with pottery	–	TFW: 5th c. CE AM: 3rd–4th c. CE (AM 14) PW: 3rd–4th c. CE (N. Syria mortar) CW: 3rd c. CE (CW 34)	Late Roman
2c	a layer of brown earth with fragments of plaster and pottery	–	TFW: – AM: 3rd–4th c. CE (AM 14) PW: 3rd–4th c. CE (N. Syria mortar) CW: 3rd c. CE (CW 34)	Late Roman
1b	brown/red clay layer with a small amount of pottery	–	–	–
1a	brown/red clay layer with a small amount of pottery	–	TFW: – AM: Hellenistic (CSA)/ca. 125 BCE CW: mid 2nd to mid 1st c. BCE	Late Hellenistic

AM – amphorae; TFW – table fine wares; CW – common wares

The gravel layer (layer 6/Table 3), was preserved between 8 and 40 m (Fig. 8B). In its central part it was interrupted by a later structure (Object D/Fig. 8B), which chronologically corresponds to layer 7, which contained ceramic material dating back to the Early Byzantine period (mid-5th to 7th CE; Fig. 11). In ancient times, part of the gravel layer between 13 and 15 m was covered with mortar and reused as a functional surface. This suggests that the once formed gravel deposit remained at least partially exposed and was then incorporated into the spatial organisation of the site. In other parts of the section, the gravel layer was sealed by later cultural deposits (e.g., layer 7), which contained Early Byzantine ceramic material. This indicates that the deposit was not removed or reworked to its full extent but rather was integrated into the occupational sequence – in some areas as a reused surface, and in others as a buried and undisturbed stratigraphic horizon. In the northern part of the profile, five layers were recorded and dated from the Late Hellenistic (2nd century BCE) to the modern period based on the ceramic material.

Notably, no traces of the pebble layer (layer 6) were recorded in the northern part of the profile. This absence may result from later levelling or reconstruction activities, as suggested by the character of layer 3 and its chronologically mixed ceramic assemblage (Early Roman to Early Byzantine periods, i.e., late 1st c. BCE to 5th c. CE). The spatially limited extent of the gravel deposit (recorded only between 8 and 40 m of the profile) supports the interpretation of a high-energy deposition restricted to a localised impact zone – potentially resulting from a tsunami wave. Several artefacts were also uncovered, indicating scattered human activity dating mainly from pottery. Based on ceramic material from layer 7, it was dated to the Early Byzantine period (mid-5th to 7th century CE). Other artefacts found in layer 2C, as well as fragments of CW34 kitchenware from south Bekaa Valley were dated to the Late Roman period (3rd–4th century CE).

An analysis of the layer system led to the conclusion that layer 6, considered a probable trace of the palaeotsunami, directly rests on layers 2b and 3 (Fig. 8B), which were dated by pottery to no later than the 3rd–4th century CE (layer 2b) or 3rd–5th century CE (layer 3). Furthermore, ceramic material found above and below layer 6 places its formation between the 3rd/4th and the 7th centuries CE. Unfortunately, no radiocarbon dating has been conducted for the gravel layer, due to the absence of preserved organic material. The chronological attribution of this deposit is therefore based exclusively on the ceramic assemblages from the directly overlying and underlying layers. Although this constitutes a limitation, the diagnostic character of the ceramic types allows for a relatively reliable chronological framework.

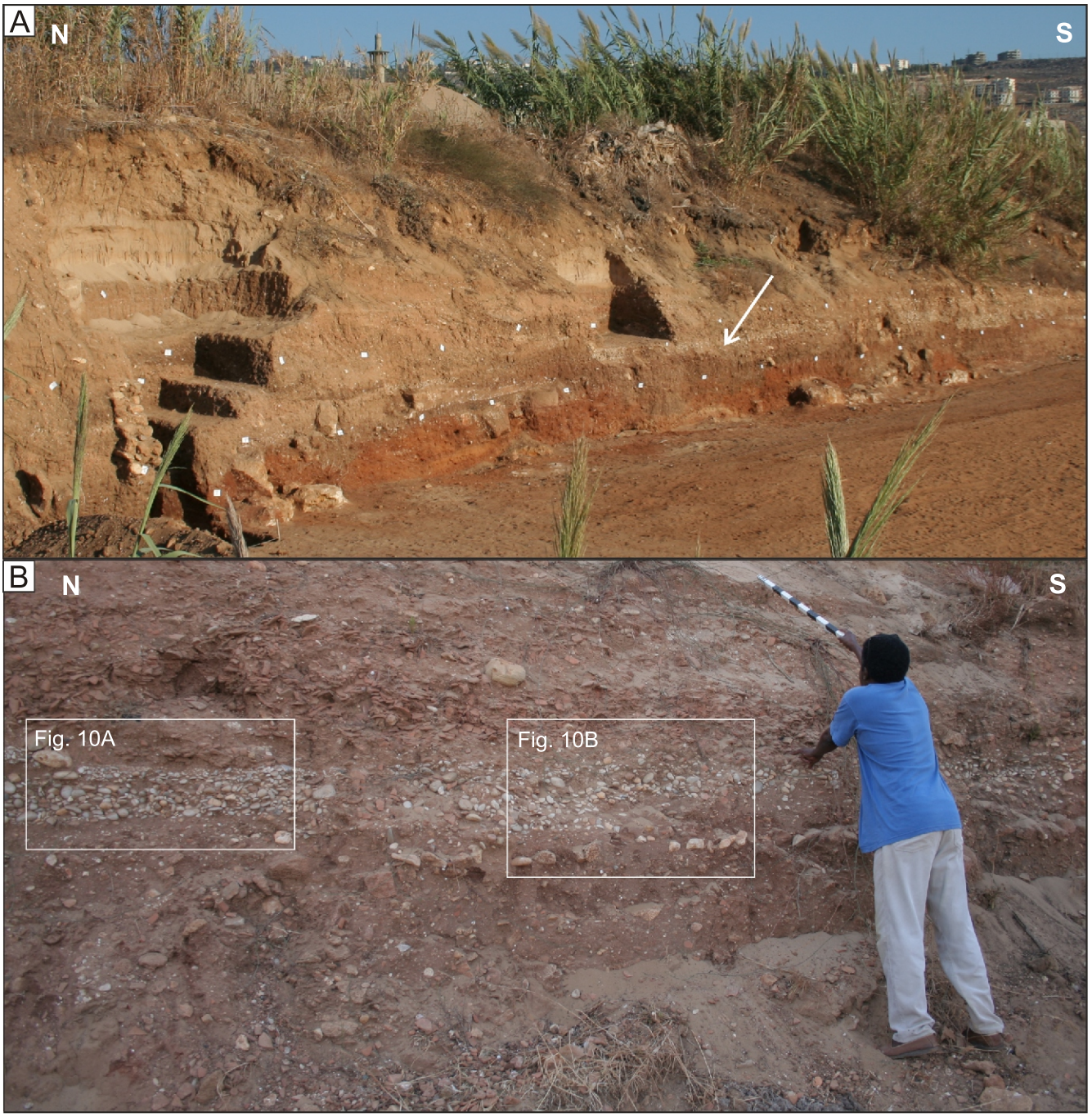

Fig. 9A – general view of the archaeological Porphyreon site, marked as a box on Figure 8B (in 2005), white arrow points to the gravelly section studied before cutting and cleaning; B – the close-up of the section studied; note the white-gravel layer inside the ceramic-bearing higher and lower layers; for details of the boxed areas see Figure 10

DISCUSSION

This section synthesises historical, geological and archaeological evidence to evaluate the plausibility of tsunami impact at Porphyreon, with particular focus on the 551 CE event. By correlating numerical modelling results with documented seismicity and site-level evidence, we aim to clarify the most likely scenario for mid-sixth-century disruption.

Correlation of numerical modelling with historical data. According to our modelling results (see Figs. 7 and 12) 12 out of the 42 analysed cases involving M7 earthquakes could potentially have impacted the densely urbanised southern coast of Cyprus and the south-eastern Mediterranean coast. Among the earthquake events analysed, scenarios 30 and 31, both associated with the Mount Lebanon Thrust, show the greatest alignment with historical data. These events could be correlated with the 551 CE earthquake, which we propose as the most probable cause of destruction at Porphyreon. This correlation is based on the spatial proximity of fault segments 30 and 31 to the Porphyreon site, the matching height and reach of the modelled tsunami wave (up to 2.6 m), and the consistency of the event's date with the archaeological gap and gravel layer at the site. It is supported by arguments regarding the extent of the tsunami and the proximity of the fault to cities such as Berytus,

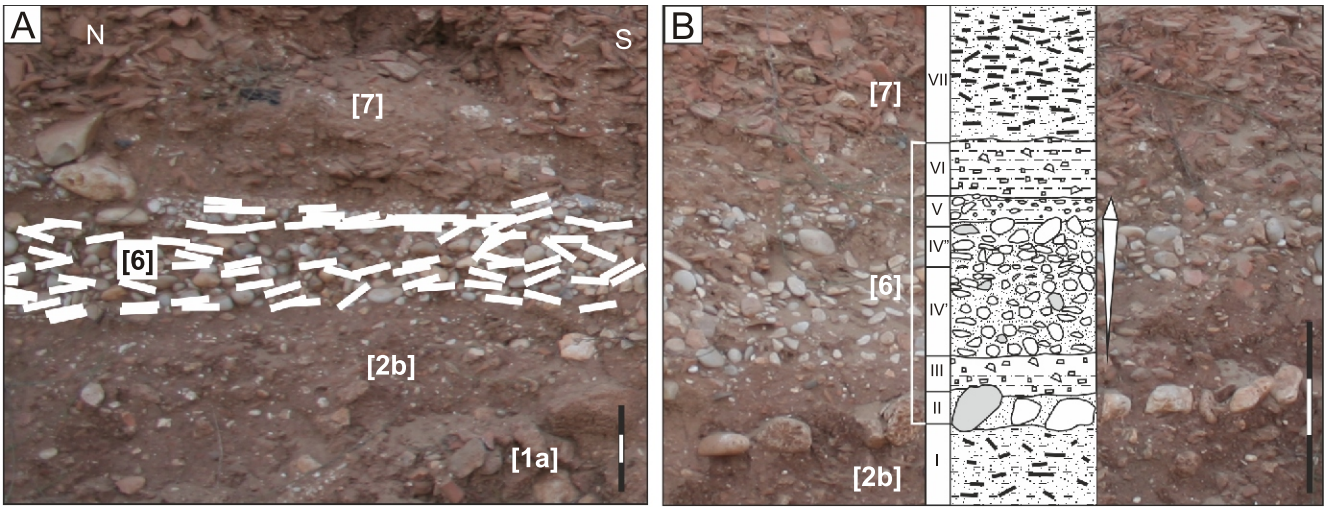

Fig. 10A – elongation of the longer axes of the flat pebbles, number in bracket – identified archaeological layers from Figure 8B; B – details of the gravelly succession studied; I–VII depositional layers identified within archaeological layers numbered 2b, 6 and 7

For explanation and interpretation – see text. The length of the vertical scale is 30 cm

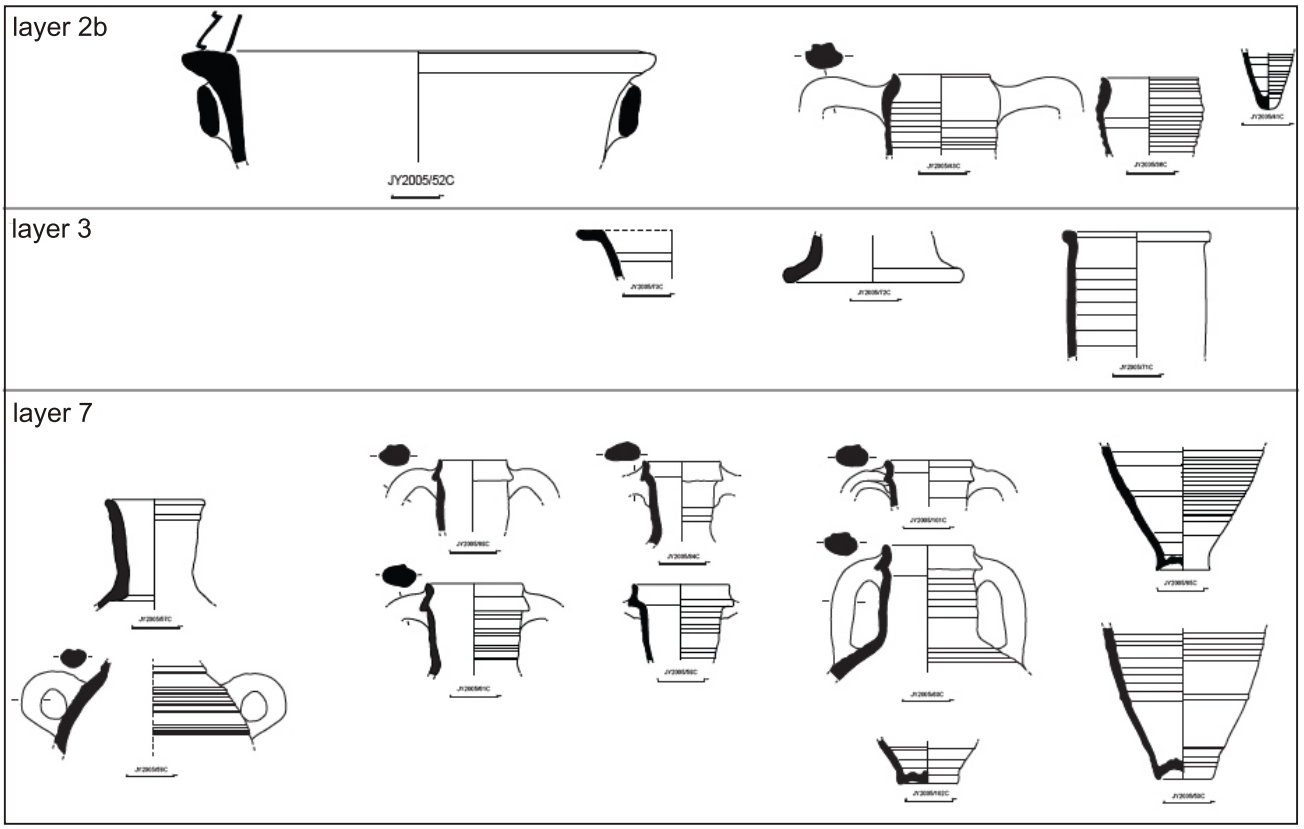

Fig. 11. Characteristic ceramic vessel forms and types to allow dating of layers 2b, 3 and 7 in the section studied

The ceramic vessel forms found in layers 1 to 5 date to the period from the Early Roman to Early Byzantine periods (late 1st c. BCE to 5th c. CE). Layer 7, corresponding to the accumulation of material above pebble layer 6 proposed as a tsunami trace, contained vessels dating back to the Early Byzantine period (mid 5th to 7th CE). Layer 6, visualised on the stratigraphic profile, therefore separates two groups of vessel forms of distinctly different dates

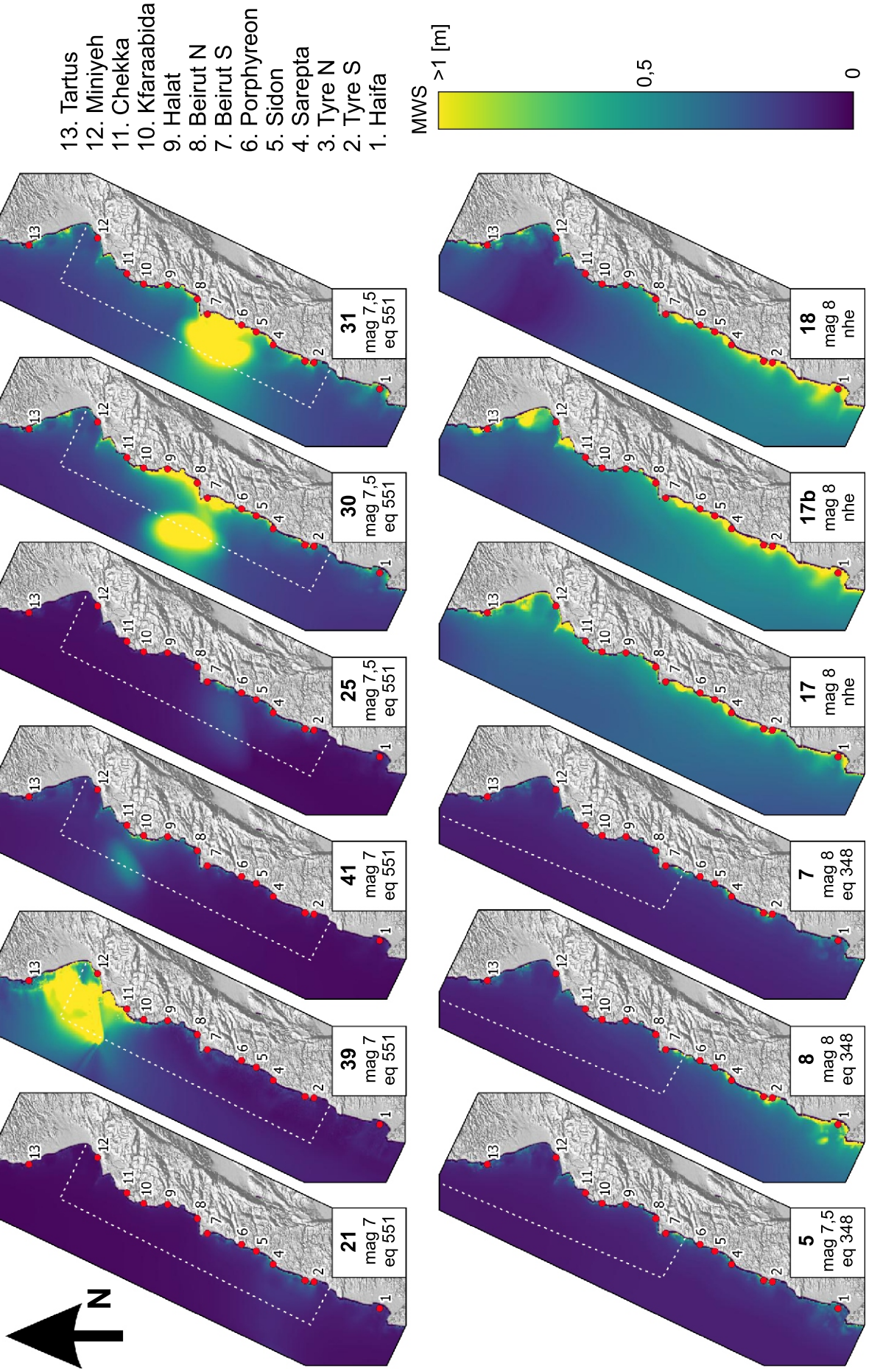

Fig. 12. The maximum height of the wave off the Lebanese coast; the dots indicate the coastal localities for which the height of the tsunami wave as a function of time was calculated (calculations in Staniszewski et al., 2025)

The white dashed line shows the historical extent of the wave that the earthquake caused in 551and 348 CE; nhe – never happened earthquake

Table 4

List and description of structures A–F in Figure 8B

Object	Layer	Metres*	Description	Non-ceramic material	Layer dating
A	3, 4, 5	15.5–2.5	section of vertical wall	–	Late Hellenistic to Early Roman mid 2nd to the late of 1st BCE
B	2a, 3, 4	8	horizontal wall?/platform?	–	Late Hellenistic to Early Roman mid 2nd to the late of 1st BCE
C	3	11–12	kiln	–	Late Hellenistic to Early Roman mid 2nd to the late of 1st BCE
D	7, crosses layer 6	22–24	two vertical walls with plaster	–	Early Byzantine (mid 4th to early 7th)
E	1, 2c/1	38.5–41.5	dark brown layer of soil with small fragments of pottery, burning and small stones	–	Late Roman (late 3rd to mid 4th CE)
E	1, 2c/2	38.5–41.5	very compact light brown layer with ceramic fragments	–	Late Roman (late 3rd to mid 4th CE)
E	1, 2c/3	38.5–41.5	soil mixed with a lot of pottery fragments	–	Late Roman (late 3rd to mid 4th CE)
F	2c	41.5–43	Kiln; dark brown layer of earth	Pottery wasters	Late Roman (late 3rd to mid 4th CE)

* – metres along the cross-section from Figure 8B

Sidon and Tyre, where archaeological and historical data corroborate that earthquake tremors were experienced (Darawcheh et al., 2000). Elias et al. (2007) state that the evidence supports the interpretation that the earthquake event in 551 CE was tsunamigenic. In addition, the epicentre of the 551 CE earthquake correlates with the location described by Ambraseys (2009; represented in our models as faults 30 and 31). Plassard and Kogoj (1981), Ambraseys and Synolakis (2010) and Salamon et al. (2024) also correlated the 551 CE earthquake to the Mount Lebanon Thrust; however, they located it in the northern part of the slip (corresponding to our model scenarios 33 and 36). Based on historical data describing the occurrence of the 551 CE tsunamis, our interpretation presents a more plausible scenario compared to that proposed by Plassard and Kogoj (1981) and Ambraseys and Synolakis (2010). However, Faysal et al. (2023) highlighted that the Latakia Ridge, with its prominent seafloor feature, may well be the most active structure offshore Lebanon and was likely the source of the 9 July 551 CE tsunamigenic earthquake. However, these assumptions are based on 3D seismic interpretation of the major and minor faults offshore Lebanon, without modelling the extent of the tsunami impact. Moreover, Faysal et al. (2023) concluded, based on an analysis of existing literature, that the tsunami that occurred in 551 CE was caused by an earthquake with a magnitude of 7.2. In contrast, our modelling indicates that for the faults associated with Latakia Ridge to generate a tsunami wave height above 1 metre in the Porphyreon area, it would have to have a magnitude above 8.

Similar to Sieberg (1932) and Antonopoulos (1980), we have found no evidence that the earthquake of 348 CE would generate a tsunami capable of reaching Berytus (see Fig. 7 and Table 2). Based on our models, it should be emphasised that in scenario 8, considering a M8 earthquake, a tsunami wave reached Tyre and Sidon with sufficient energy to cause significant impact on this area. Both the scenarios describing the events of 342 CE and ~300 CE did not indicate the possibility of a tsunami threatening the coast of Lebanon. However, one of our scenarios for 342 CE yields very similar results to the modelling of the 1222 CE earthquake (Yolsal et al., 2007), demonstrating the applicability of our modelling approach in predicting and determining geohazards associated with historical tsunami impacts.

In addition to the modelled scenarios, we also considered other major catastrophic events, such as the 365 CE earthquake off the coast of Crete. However, we did not model this event since it was included in the models proposed by England et al. (2015) and Ott et al. (2021). According to their scenarios, it can be concluded that such an event did not impact the Porphyreon site. For the other tsunami episodes investigated, it was challenging to establish a consistent explanation that aligned the modelled earthquake scenarios with the presence of the gravel layer and observed damage at Porphyreon. Some cases showed correlation with historical tsunami events, while in others, Porphyreon's inundation was recorded, but lacked confirmation in the epigraphic record or correlation with known historical events. Among the scenarios considered, those associated with the Cyprus subduction zone align with the observed destruction at the site. However, events of such scale would have affected the entire region. To date, no historical indications have been found of an event in which such a large portion of the coastline was inundated.

Tsunami origin of the gravel layer. While our primary hypothesis favours a tsunami origin, we also considered alternative explanations such as storm surge deposition or anthropogenic infill. However, the internal sedimentary structures – including grading, an erosional base, and the lack of compaction – do not align with typical storm deposits or construction layers. Furthermore, the absence of architectural elements, prepared ground surfaces, or consistent spatial patterning reduces the likelihood of human agency. Nonetheless, we acknowledge that without direct sedimentological analyses, these alternative scenarios cannot be ruled out entirely. Given all the above considerations, we cannot exclude the possibility that the event described here was caused by a tsunami not mentioned in any written source of the period. We also allow for the possibility that such an event occurred as a result of a catastrophic torrential storm, but our geological interpretation of the record makes such a possibility highly unlikely in our opinion based on current evidence with preserved sedimentary features that better match tsunami-related processes.

Despite the lack of more detailed sedimentological analyses, our interpretation is that the observed sequence (see section 'Sedimentological interpretations') was formed in a single depositional event of varying intensity, potentially associated

with the propagation of a tsunami wave onto the coastal region. The gravel layer exhibits features similar to those interpreted as Holocene tsunami-related coastal beach and dune deposits, as described by researchers such as Nichol et al. (2003), Nanayama and Shigeno (2006), Hawkes et al. (2007), Morton (2008) and Yu et al. (2020). These features include a sharp erosional basal contact, an upwards-fining and upwards-coarsening sequence, sand sheets, gravel fabric, and a sheet of gravel with cobble-sized clasts. However, Shanmugam (2012) argued that there is no definite evidence for tsunami-related deposits in the coastal-beach environment. According to Shanmugam (2012), incoming tsunami waves (landward) and outgoing backwash flows (seaward) can trigger a variety of processes, making it challenging to establish reliable sedimentological criteria for distinguishing palaeo-tsunami deposits in various environments. However, this interpretation remains hypothetical in the absence of direct sedimentological evidence.

The hypothesis that the gravel layer originated from river flooding can be reasonably excluded. Had such a flood occurred in 551 CE, it would likely have caused widespread destruction to overlying structures, including the Byzantine Basilica yet no such damage is evident in the archaeological record. Moreover, the absence of major river systems in the immediate vicinity significantly weakens this interpretation. While a periodically active braided stream could theoretically have deposited such sediments, this would imply a recurrent geomorphological process rather than a singular event. In that case, one would expect repeated episodes of deposition and destruction, which are not reflected in the archaeological or stratigraphic record at the site.

Integrating archaeological and seismological evidence. The comparison between seismological and archaeological data concerning the ancient city of Porphyreon reveals several inconsistencies. The stratigraphic profile cited in this study appears clear and suggests the possibility of a correlation between the archaeological data and the 551 CE earthquake and subsequent tsunami selected for its potential impact on the Porphyreon area, and their alignment with historical and geological evidence. This analysis contributes to a better understanding of the settlement's evolution. Tsunami wave height models indicated that, in some scenarios, waves may have reached heights of up to 2.6 m. Consequently, it is plausible that the encroachment of tsunami waves onto the shoreline could have caused the destruction of a coastal settlement such as Porphyreon. Layer 6 at Porphyreon is interpreted as resulting from the 551 CE tsunami; however, evidence of tsunami impact is not uniformly distributed across the site, particularly in areas with residential buildings and the Basilica. This inconsistency may be attributed to several factors:

- localised depositional patterns: tsunamis often deposit materials unevenly, influenced by local topography and pre-existing structures, which may protect certain areas while exposing others to more significant deposition;
- excavation limitations: the scope of our archaeological excavations was limited, and it is possible that tsunami-related deposits were present but not uncovered in the excavated sections;
- post-depositional disturbances: subsequent human activities, such as rebuilding, or natural erosion processes, could have disturbed or removed sedimentary evidence of the tsunami, particularly in areas with significant later construction;
- variability in tsunami intensity: the intensity and impact of the tsunami waves may have varied across the site, potentially leaving less detectable traces in some areas.

Given these considerations, more extensive remote sensing and geophysical surveys and archaeological excavations are needed to fully understand the impact of the 551 CE tsunami across the entire site. Moreover, the large surviving fragments of Porphyreon's residential buildings (Fig. 8A), situated at a height of ~10 m a.s.l. and at a distance of no more than 100 m from the seashore, show no clear signs of destruction. Similarly, the Byzantine Basilica, which functioned in the 5th–6th centuries CE directly on the seashore at a height of only 4 m a.s.l., also lacks architectural evidence of tsunami-related destruction. To date, no architectural traces indicative of seismic damage (e.g. wall cracks, collapsed structures or subsequent rebuilding) have been documented in the excavated sectors. This absence of evidence may also reflect later human modifications of the archaeological layers, particularly during the Byzantine period. These transformations are well documented stratigraphically, though without clear architectural evidence of post-seismic repair or rebuilding. No written records specifically describing tsunami-related destruction at Porphyreon have been preserved, though historical sources document coastal damage in other Phoenician cities following the 551 CE event. Instead, the archaeological record reveals an intriguing gap between an earlier settlement that functioned on the same site until the 2nd–3rd centuries CE and the Late Antique settlement constructed atop its remains during the late 4th and 5th centuries CE. The abandonment of the earlier settlement and subsequent reconstruction could correlate with the possible effects of the 4th century CE earthquakes, rather than the well-documented 551 CE event.

Holocene shoreline uplift. There has been long-standing scholarly discussion regarding the shoreline uplift in Lebanon and the processes responsible for it (e.g., Sanlaville, 1977; Pirazzoli et al., 1991; Elias et al., 2007). Some researchers believe that it is related, among other things, to Holocene sea-level fluctuations (Sanlaville, 1977), while others link them to the tectonic activity (e.g., Elias et al., 2007), including the 551 CE earthquake and subsequent seismic events.

A significant contribution to this discussion is the study by Morhange et al. (2006), which identified two main Holocene regional crustal uplift phases over the past 6000 years along the Lebanese coast: (i) an upper shoreline at ~+1.2 to +1.4 m, which lasted from ~4,050 BCE to 1,050 BCE and (ii) a lower shoreline at +0.8 ±0.4 m, developed between 750 BCE and the 6th century CE, coinciding with the so-called "Early Byzantine Tectonic Paroxysm" (*sensu* Pirazzoli, 1986). A relative stabilisation to modern sea levels took place ~1,000 CE (Morhange et al., 2006). These uplifted coastal features have been interpreted by Morhange et al. (2006) as resulting from the activation of the Yammouneh and the Roum-Tripoli thrusts, as well as slip along transverse faults. Building on this, Faysal et al. (2023) argued that the regional uplift documented by Morhange et al. (2006) may be better explained by the results of the major tectonic role of the Latakia Ridge in the eastern Mediterranean, and suggested that the uplifts documented in Morhange et al. (2006) could be due to the transpressional structures mapped by Faysal et al. (2023) mapped along the Lebanese margin, and that the last uplift, contemporaneous with the 551 CE earthquake, may have resulted from an earthquake that could have been triggered along the Lebanese margin by a major event that occurred along the Latakia ridge. However, our results indicate that faults other than those associated with the Latakia Ridge were responsible for generating the 551 CE tsunami. For this reason, the course of this event and its uplift mechanism in our opinion is questionable and that is why we have not included it in any of our analyses.

Morhange et al. (2006) also note regional uplift intensity, reporting a decrease near Beirut and increases again in the Saida region (+0.5 m) compared to northern Lebanon. This pattern is particularly relevant to our site: the Byzantine Basilica at Porphyreon, which is today located directly on the seashore at an elevation of just 4 m a.s.l., shows no signs of tsunami-related destruction. This observation allows us to constrain the maximum inundation height of the tsunami in this area. Even accounting for possible uplift of up to 0.5 m, the maximum inundation of the tsunami could only have reached areas situated below 3.5 m a.s.l. Taking all these factors into account including the absence of structural damage to the Basilica, the limited maximum uplift in the Porphyreon area –0.5 m, and our modelling results for tsunami wave based on our modelling was 0.1 m (342 CE), 0.5 m (348 CE) and 2.6 m (551 CE) we conclude that our proposed tsunami scenario for the 551 CE event is highly plausible.

CONCLUSIONS

Based on 135 earthquake scenarios for >M7 events, distributed across a total of 42 faults located in the south-eastern Mediterranean, we infer the following patterns of tsunami risk: for the 342 CE earthquake, only the fault southwest of the Cyprus coast could potentially have posed a credible threat to the Lebanese coast; for the 348 CE earthquake, the greatest hazard can be associated with an oblique-slip fault in the central part of the Levantine Basin. In the case of the 551 CE earthquake, multiple faults represent potential tsunami sources, but the greatest risk appears linked to faults associated with the Mount Lebanon and Tripoli-Beirut thrust systems.

In our study, numerical modelling results were integrated with sedimentological observations and archaeological data. Based on the characteristics of the gravel layer embedded within the cultural layers at the Porphyreon, it was determined that the section studied was formed during a single high-energy depositional episode of changing intensity, likely associated with tsunami waves propagating onto the land area. The calculated maximum tsunami wave height modelled for 551 CE event in the Porphyreon area reached 2.6 m. Accordingly, the 551 CE tsunami is considered to be the most plausible trigger for the formation of the gravel layer observed within the cultural strata of the Porphyreon archaeological site. Although the tsunami origin of the deposit cannot be conclusively confirmed due to the absence of direct sedimentological and geochronological data, the stratigraphic and archaeological context support it as the most plausible scenario currently available. Should access to the site become feasible in the future – pending improvement of political situation in the region – further research incorporating direct sedimentological sampling and geochemical analysis will be essential to further evaluate the tsunami hypothesis against alternative depositional scenarios, including storm-induced and anthropogenic processes.

Our numerical modelling results also provided some relevant insights to future risk assessment. Tectonic zones previously associated with high-magnitude seismic activity may continue to pose significant threat to coastal populations. Notably, there is no historical documentation of a tsunami event associated with the Cyprus subduction zone that resulted in widespread coastal inundation. Nevertheless, the potential for such an event should not be dismissed particularly given that this zone extends further into Turkey and Syria, where a devastating 7.8 magnitude earthquake occurred on 6th February 2023.

Acknowledgements. The research presented in this article is based on an archaeological project conducted by a Polish-Lebanese team representing the University of Warsaw, the Polish Academy of Sciences, and the General Directorate of Antiquities, conducted between 2003 and 2014 in Porphyreon, Lebanon. Fieldwork was financially supported by the Polish Centre of Mediterranean Archaeology of the University of Warsaw and the Ministry of Science and Higher Education of the Republic of Poland. Geological observations at the Porphyreon site, conducted in 2021, were funded by the Faculty of Geology and the Polish Centre of Mediterranean Archaeology, both affiliated with the University of Warsaw. We would like to express our sincere gratitude to Dr Krzysztof Domżalski from the Institute of Archaeology and Ethnology, Polish Academy of Science, for providing the chronological information on the Table Fine Wares.

REFERENCES

[dataset] USGS Earthquake Catalogue, 2021; https://earthquake.usgs.gov/ (accessed in 2022)

Aki, K., 1966. Generation and propagation of G-waves from the Niigata earthquake of June 16, 1964. Part. 2. Estimation of earthquake moment, released energy, and stress-strain drop from G-wave spectrum. Bulletin of the Earthquake Research Institute, University of Tokyo, **44:** 73–88.

Aksu, A.E., Hall, J.,Yaltýrak, C., 2021. Miocene-Quaternary tectonic, kinematic and sedimentary evolution of the eastern Mediterranean Sea: A regional synthesis. Earth-Science Reviews, **220,** 103719; https://doi.org/10.1016/j.earscirev.2021.103719

Altinok, Y., Alpar, B., Özer, N., Aykurt, H., 2011. Revision of the tsunami catalogue affecting Turkish coasts and surrounding regions. Natural Hazards Earth System Sciences, **11:** 273–291; https://doi.org/10.5194/nhess-11-273-2011

Ambraseys, N.N., 1962. Data for the investigation of the seismic sea waves in the Eastern Mediterranean. Bulletin of the Seismological Society of America, **52:** 895–913; https://doi.org/10.1785/BSSA0520040895

Ambraseys, N., 2005. Archaeoseismology and Neocatastrophism. Seismological Research Letters, **76**: 560–564; https://doi.org/10.1785/gssrl.76.5.560

Ambraseys, N., 2009. Earthquakes in the Mediterranean and Middle East: A Multidisciplinary Study of Seismicity up to 1900. Cambridge University Press. Cambridge, United Kingdom; https://doi.org/10.1785/gssrl.76.5.560

Ambraseys, N., Synolakis, C., 2010. Tsunami catalogs for the Eastern Mediterranean, revisited. Journal of Earthquake Engineering, **14**: 309–330; https://doi.org/10.1080/13632460903277593

Antonopoulos, A., 1987. Contribution to the knowledge of tsunamis in the Eastern Mediterranean from ancient times until the recent. Annales Géologiques des Pays Helléniques, **29**: 740–757.

Antonopoulos, J., 1980. Data from investigation on seismic sea-waves events in the Eastern Mediterranean from the birth of Christ to 500 AD. Annali di Geofisica, **33:** 141–161.

Barbano, M.S., Castelli, V., Pantosti, D., Pirrotta, C., 2014. Integration of historical, archaeoseismic and paleoseismological data for the reconstruction of the early seismic history in

Messina Strait (south Italy): the 1st and 4th centuries AD earthquakes, Annals of Geophysics, **57,** S0192; https://doi.org/10.4401/ag-6369

Bardy, G., 1958. Eusèbe de Césarée. Histoire ecclésiastique, III: Livres VIII-X et les martyrs en Palestine (Sources Chrétiennes N°55). Éditions du Cerf. Paris.

Bowman, S.A., 2011. Regional seismic interpretation of the hydrocarbon prospectivity of offshore Syria. GeoArabia, **16:** 95–124; https://doi.org/10.2113/geoarabia160395

Brax, M., Albini, P., Beauval, C., Jomaa, R., Sursock, A., 2019. An Earthquake Catalog for the Lebanese Region. Seismological Research Letters, **90:** 2236–2249; https://doi.org/10.1785/0220180292

Bruins, H.J., MacGillivray, J.A., Synolakis, C.E., Benjamini, C., Keller, J., Kisch, H.J., Kleugel, A., van der Plicht, J., Klügel, A., 2008. Geoarchaeological tsunami deposits at Palaikastro (Crete) and the Late Minoan IA eruption of Santorini. Journal of Archaeological Science, **35**: 191–212; https://doi.org/10.1016/j.jas.2007.08.017

Carton, H., Singh, S.C., Tapponnier, P., Elias, A., Briais, A., Sursock, A., Jomaa, R., King, G.C., Daëron, M., Jacques, E., Barrier, L., 2009. Seismic evidence for Neogene and active shortening offshore of Lebanon (Shalimar cruise). Journal of Geophysical Research, **114:** B07407; https://doi.org/10.1029/2007JB005391

Darawcheh, R., Sbeinati, M.R., Margottini, C., Paolini, S., 2000. The 9 July 551 A.D. Beirut earthquake, Eastern Mediterranean region. Journal of Earthquake Engineering, **4:** 403–414.

Dey, H., Goodman-Tchernov, B., 2010. Tsunamis and the port of Caesarea Maritima over the longue durée: a geoarchaeological perspective. Journal of Roman Archaeology, **23:** 265–284; https://doi.org/10.1017/S1047759400002397

Dey, H., Goodman-Tchernov, B., Sharvit, J., 2014. Archaeological evidence for the tsunami of January 18, A.D. 749: a chapter in the history of Early Islamic Qâysariyah (Caesarea Maritima). Journal of Roman Archaeology, **27:** 357–373; https://doi.org/10.1017/S1047759414001287

Donzé, F., Mora, P., Magnier, S-A., 1994. Numerical simulation of faults and shear zones. Geophysical Journal International, **116:** 46–52; https://doi.org/10.1111/j.1365-246X.1994.tb02126.x

Dutykh, D., Poncet, R., Dias, F., 2011. The VOLNA code for the numerical modeling of tsunami waves: Generation, propagation and inundation. European Journal of Mechanics B/Fluids, **30:** 598–615; https://doi.org/10.1016/j.euromechflu.2011.05.005

Elias, A., Tapponnier, P., Singh, S.C., King, G.C.P., Briais, A., Daëron, M., Carton, H., Sursock, E., Jomaa, R., Klinger, Y., 2007. Active thrusting offshore Mount Lebanon: source of the tsunamigenic A.D. 551 Beirut-Tripoli earthquake. Geology, **35:** 755–758; https://doi.org/10.1130/G23631A.1

England, P., Howell, A., Jackson, J., Synolakis, C., 2015. Palaeotsunamis and tsunami hazards in the Eastern Mediterranean. Philosophical Transactions of the Royal Society A: Mathematical, Physical and Engineering Sciences, **373**, 20140374; https://doi.org/10.1098/rsta.2014.0374

Erdik, M., Şeşetyan, K., Demircioğlu, M.B., Harmandar, E., 2014. Assessment of site-specific earthquake hazard for Bisri dam, Lebanon. Report for the Council for development and reconstruction of the Republic of Lebanon. Boğaziçi University, Kandilli Observatory and Earthquake Research Institute, Department of Earthquake Engineering.

Falvard, S., Paris, R., 2017. X-ray tomography of tsunami deposits: Towards a new depositional model of tsunami deposits. Sedimentology, **64:** 453–477; https://doi.org/10.1111/sed.12310

Faysal, R., Nemer, T., Sarieddine, K., 2023. Investigating the geological fault framework offshore Lebanon: insight into the earthquake geology of the eastern Mediterranean region. Pure and Applied Geophysics, **180:** 3249–3268; https://doi.org/10.1007/s00024-023-03336-5

Frendo, J.D., 1975. The histories / Agathias. Walter de Gruyter, Berlin.

Fernández-Blanco, D., Mannu, U., Giovanni Bertotti, G., Willett, S.D., 2020. Forearc high uplift by lower crustal flow during growth of the Cyprus-Anatolian margin. Earth and Planetary Science Letters, **544**, 116314; https://doi.org/10.1016/j.epsl.2020.116314

Fischer, P., Finkler, C., Röbke, B. R., Baika, K., Hadler, H., Willershäuser, T., Vött, A., 2016. Impact of Holocene tsunamis detected in lagoonal environments on Corfu (Ionian Islands, Greece): Geomorphological, sedimentary and microfaunal evidence. Quaternary International, **401:** 4–16; https://doi.org/10.1016/j.quaint.2015.07.019

Fokaefs, A., Papadopoulos, G., 2007. Tsunami hazard in the Eastern Mediterranean: strong earthquakes and tsunamis in Cyprus and the Levantine Sea. Natural Hazards, **43**: 503–526; https://doi.org/10.1007/s11069-006-9011-3

Geist, E.L., Bilek, S.L., 2001. Effect of depth-dependent shear modulus on tsunami generation along subduction zones. Geophysical Research Letters, **28:** 1315–1318; https://doi.org/10.1029/2000GL012385

Geyer, P., (ed.), 1965. Antonini Placentini Itinerarium, in Itineraria et alia geographica (Corpus Chistianorum, series Latina 175–176). Turnholti: Typographi Brepols editores pontificii, 129–174.

Goodman-Tchernov, B.N., 2020. Archaeological dating of tsunami and storm deposits. In: Geological Records of Tsunamis and Other Extreme Waves (eds. M. Engel, J. Pilarczyk, S.M. May, D. Brill and E. Garrett): 729–743. Elsevier; https://doi.org/10.1016/B978-0-12-815686-5.00033-X

Goodman-Tchernov, B.N., Dey, H.W., Reinhardt, E.G., McCoy, F., Mart, Y., 2009. Tsunami waves generated by the Santorini eruption reached Eastern Mediterranean shores. Geology, **37:** 943–946; https://doi.org/10.1130/G25704A.1

Guidoboni, E., Comastri, A., Traina, G., 1994. Catalogue of Ancient Earthquakes in the Mediterranean Area up to the 10th Century. Instituto Nazionale di Geofisica, Rome.

Hall, L.J., 2004. Roman Berytus: Beirut in Late Antiquity. Routledge, London and New York; https://doi.org/10.4324/9780203499078

Harrison, R.W., Tsiolakis, E., Stone, B.D., Lord, A., McGeehin, J.P., Mahan, S.A., Chirico, P., 2013. Late Pleistocene and Holocene uplift history of Cyprus: implications for active tectonics along the southern margin of the Anatolian microplate. Geological Society Special Publications, **372:** 561–584; https://doi.org/10.1144/SP372.3

Hawie, N., Gorini, C., Deschamps, R., Nader F.H., Montadert, L., Granjeon, D., Baudin, F., 2013. Tectono-stratigraphic evolution of the northern Levant Basin (offshore Lebanon). Marine and Petroleum Geology, **48:** 392–410; https://doi.org/10.1016/j.marpetgeo.2013.08.004

Hawie, N., Deschamps, R., Granjeon, D., Nader, F.D., Gorini, C., Muller, C., Montadert, L., Baudin, F., 2017. Multi-scale constraints of sediment source to sink systems in frontier basins: a forward stratigraphic modelling case study of the Levant region. Basin Research, **29:** 418–445; https://doi.org/10.1111/bre.12156

Hawkes, A.D., Bird, M., Cowie, S., Grundy-Warr, C., Horton, B.P., Hwai, A.T.S., Law, L., Macgregor, C., Nott, J., Ong, J.E., Rigg, J., Robinson, R., Tan-Mullins, M., Sa, T.T., Yasin, Z., Aik, L.W., 2007. Sediments deposited by the 2004 Indian Ocean Tsunami along the Malaysia–Thailand Peninsula. Marine Geology, **242:** 169–190; https://doi.org/10.1016/j.margeo.2007.02.017

Heinrich, P., Piatanesi, A., Hébert, H., 2001. Numerical modelling of tsunami generation and propagation from submarine slumps: the 1998 Papua New Guinea event. Geophysical Journal International, **145:** 97–111; https://doi.org/10.1111/j.1365-246X.2001.00336.x

Hill, T.P., 2022. On the oval shape of beach stones. AppliedMath, **2:** 16–38; https://doi.org/10.3390/appliedmath2010002

Hoffmann, N., Master, D., Goodman-Tchernov, B., 2018. Possible tsunami inundation identified amongst 4–5th century BCE archaeological deposits at Tel Ashkelon, Israel. Marine Geology, **396:** 150–159; https://doi.org/10.1016/j.margeo.2017.10.009

Ismail-Zadeh, A., Soloviev, A., 2022. Numerical Modelling of Lithospheric Block-and-Fault Dynamics: What Did We Learn About Large Earthquake Occurrences and Their Frequency? Surveys in Geophysics, **43:** 503–528; https://doi.org/10.1007/s10712-021-09686-w

Kinnaird, T., Robertson, A., 2013. Tectonic and sedimentary response to subduction and incipient continental collision in southern Cyprus, easternmost Mediterranean region. Geological Society Special Publications, **372:** 585–614; https://doi.org/10.1144/SP372.10

Konon, A., Nadimi, A., Koprianiuk, M., Wysocka, A., Szaniawski, R., Wyglądała, M., Słaby, E., Beygi, S., Barski, M., 2016. Formation of intracontinental basins in the opposite corners of the Tabas block as coeval structures controlled by transpressional faulting, Iran. GSA Bulletin, **128:** 1593–1617; https://doi.org/10.1130/B31362.1

Krumbein, W.C., 1941. Measurements and geological significance of shape and roundness of sedimentary particles. Journal of Sedimentary Research, **11:** 64–72; https://doi.org/10.1306/D42690F3-2B26-11D7-8648000102C1865D

Lemenkova, P., 2021. Submarine tectonic geomorphology of the Pliny and Hellenic Trenches reflecting the geological evolution of southern Greece. Rudarsko Geolosko Naftni Zbornik, **36:** 33–48; https://doi.org/10.17794/rgn.2021.4.4

Liritzis, I., Westra, A., Miao, C., 2019. Disaster Geoarchaeology and Natural Cataclysms in World Cultural Evolution: an overview. Journal of Coastal Research, **35**: 1307–1330; https://doi.org/10.2112/JCOASTRES-D-19-00035.1

Luis, J.F., 2007. Mirone: a multi-purpose tool for exploring grid data. Computers & Geosciences, **33:** 31–41; https://doi.org/10.1016/j.cageo.2006.05.005

Malalas, I., 2000. Ioannis Malalae Chronographia. Walter De Gruyter, Berlin.

Mansinha, L., Smylie, D.E., 1971. The displacement fields of inclined faults. Bulletin of the Seismological Society of America, **61:** 1433–1440; https://doi.org/10.1785/BSSA0610051433

Maramai, A., Brizuela, B., Graziani, L., 2014. The Euro-Mediterranean Tsunami Catalogue. Annals of Geophysics, **57:** S0435; https://doi.org/10.4401/ag-6437

Marriner, N., Pirazzoli, P., 2006. Evidence of late Holocene tsunami events in Lebanon. Zeitschrift für Geomorphologie, **146:** 81–95.

Marriner, N., Morhange, C., Doumet-Serhal, C., 2006. Geoarchaeology of Sidon's ancient harbours, Phoenicia. Journal of Archaeological Science, **33:** 1514–1535; https://doi.org/10.1016/j.jas.2006.02.004

Marriner, N., Morhange, C., Carayon, N., 2008. Ancient Tyre and its harbours: 5000 years of human-environment interactions. Journal of Archaeological Science, **35:** 1281–1310; https://doi.org/10.1016/j.jas.2007.09.003

Meier, M., 2007. Natural disasters in the chronographia of John Malalas: reflections on their function an initial sketch. The Medieval History Journal, **10:** 237–266; https://doi.org/10.1177/097194580701000209

Mikumo, T., Miyatake, T., 1983. Numerical modelling of space and time variations of seismic activity before major earthquakes. Geophysical Journal of the Royal Astronomical Society, **74:** 559–583; https://doi.org/10.1111/j.1365-246X.1983.tb01889.x

Mordechai, L., 2020. Berytus and the aftermath of the 551 earthquake. U Schyłku Starożytności: Studia Źródłoznawcze, **17/18:** 198–241.

Morhange, C., Marriner, N., 2010. Paleo-Hazard in the Coastal Mediterranean: A Geoarchaeological Approach. In: Landscape and Societies (eds. I. Martini and W. Chesworth): 223–235. Springer, Dordrecht; https://doi.org/10.1007/978-90-481-9413-1_14

Morhange, C., Marriner, N., Pirazzoli, P.A., 2006. Evidence of Late-Holocene Tsunami Events in Lebanon. Zeitschrift für Geomorphologie, NF, **146:** 81–95.

Morhange, C., Pirazzoli, P.A., Marriner, N., Montaggioni, L.F., Nammour, T., 2006. Late Holocene relative sea-level changes in Lebanon, Eastern Mediterranean. Marine Geology, **230**: 99–114; https://doi.org/10.1016/j.margeo.2006.04.003

Morhange, C., Salamon, A., Bony, G., Flaux, C., Galili, E., Goiran, J.P., Zviely, D., 2014. Geoarchaeology of tsunamis and the revival of neo-catastrophism in the Eastern Mediterranean. La Sapienza studies on the archaeology of Palestine and transJordan. ROSAPAT, **11:** 61–81.

Morton, R.A., Goff, J.R., Nichol, S.L., 2008. Hydrodynamic implications of textural trends in sand deposits of the 2004 tsunami in Sri Lanka. Sedimentary Geology, **207:** 56–64; https://doi.org/10.1016/j.sedgeo.2008.03.008

Nader, F.H., 2014. The Geology of Lebanon. Scientific Press, Beaconsfield.

Nader, F.H., Inati, L., Ghalayini, R., Hawie, N., Daher, S.B., 2018. Key geological characteristics of the Saida-Tyr Platform along the eastern margin of the Levant Basin, offshore Lebanon: implications for hydrocarbon exploration. Oil and Gas Science and Technology, **73:** 1–22; https://doi.org/10.2516/ogst/2018045

Nanayama, F., Shigeno, K., 2006. Inflow and outflow facies from the 1993 tsunami in southwest Hokkaido. Sedimentary Geology, **187:** 139–158; https://doi.org/10.1016/j.sedgeo.2005.12.024

Nemer, T.S., Vaccari, F., Meghraoui, M., 2023. Seismic hazard assessment of the Lebanese restraining bend: a neo-deterministic approach. Pure and Applied Geophysics, **180**: 1835–1859; https://doi.org/10.1007/s00024-023-03233-x

Nichol, S.L., Lian, O.B., Carter, C.H., 2003. Sheet-gravel evidence for a late Holocene tsunami run-up on beach dunes, Great Barrier Island, New Zealand. Sedimentary Geology, **155:** 129–145; https://doi.org/10.1016/S0037-0738(02)00191-4

Nigg, V., Wohlwend, S., Hilbe, M., Bellwald, B., Fabbri, S.C., de Souza, G.F., Donau, F., Grischott, R., Strasser, M., Anselmetti, F.S., 2021. A tsunamigenic delta collapse and its associated tsunami deposits in and around Lake Sils, Switzerland. Natural Hazards, **107:** 1069–1103; https://doi.org/10.1007/s11069-021-04533-y

Omira, R., Baptista, M.A., Matias, L., Miranda, J.M., Catita, C., Carrilho, F., Toto, E., 2009. Design of a Sea-level Tsunami Detection Network for the Gulf of Cadiz. Natural Hazards and Earth System Science, **9:** 1327–1338; https://doi.org/10.5194/nhess-9-1327-2009

Ott, R.F., Wegmann, K.W., Gallen, S.F., Pazzaglia, F.J., Brandon, M. T., Ueda, K., Fassoulas, C., 2021. Reassessing Eastern Mediterranean tectonics and earthquake hazard from the 365 CE earthquake. AGU Advances, **2**, e2020AV000315; https://doi.org/10.1029/2020AV000315

Papadopoulos, G.A., Minoura, K., Imamura, F., Kuran, U., Yalçiner, A., Fokaefs, A., Takahashi, T., 2012. Geological evidence of tsunamis and earthquakes at the Eastern Hellenic Arc: correlation with historical seismicity in the eastern Mediterranean Sea. Research in Geophysics, **2**: 90–99; https://doi.org/10.4081/rg.2012.e12

Papadopoulos, G.A., Gràcia, E., Urgeles, R., Sallares, V., De Martini, P.M., Pantosti, D., González, M., Yalciner, A.C., Mascle, J., Sakellariou, D., Salamon, A., Tinti, S., Karastathis, V., Fokaefs, A., Camerlenghi A., Novikova, T., Papageorgiou, A., 2014. Historical and pre-historical tsunamis in the Mediterranean and its connected seas: Geological signatures, generation mechanisms and coastal impacts. Marine Geology, **354:** 81–109; https://doi.org/10.1016/j.margeo.2014.04.014

Papadopoulos, K., 2021. Remembering Earthquakes in the Late Antique Eastern Mediterranean. Studia Patristica. In: Papers Presented at the Eighteenth International Conference on Patristic Studies Held in Oxford 2019: 139–164.

Pirazzoli, P.A., 1986. The early Byzantine tectonic paroxysm. Zeitschrift für Geomorphologie, Supplement Issues, **62:** 31–49.

Pirazzoli, P.A., Laborel, J., Saliège, J.F., Erol, O., Kayan, I., Person, A., 1991. Holocene raised shorelines on the Hatay coasts (Turkey): palaeoecological and tectonic implications. Marine Geology, **96:** 295–311; https://doi.org/10.1016/0025-3227(91)90153-U

Plassard, J., Kogoj, B., 1981. Séismicité du Liban. Conseil National de la Recherche Scientifique, Beirut.

Reicherter, K., Michetti, A.M., Silva Barroso, P.G., 2009. Palaeoseismology: historical and prehistorical records of earthquake ground effects for seismic hazard assessment. Geological Society Special Publications, **316:** 1–10; https://doi.org/10.1144/SP316.1

Reinhardt, E.G., Goodman, B.N., Boyce, J.I., Lopez, G., van Hengstum, P., Rink, W.J., Mart, Y., Raban, A., 2006. The tsunami of 13 December A.D. 115 and the destruction of Herod the Great's harbor at Caesarea Maritima, Israel. Geology, **34:** 1061–1064; https://doi.org/10.1130/G22780A.1

Romano, V., De'Haven Hyman, J., Karra, S., Valocchi, A.J., Battaglia, M., Bigi, S., 2017. Numerical modeling of fluid flow in a fault zone: a case study from Majella Mountain (Italy). Energy Procedia, **125:** 556–560; https://doi.org/10.1016/j.egypro.2017.08.191

Salah-Eldin, A., El-Khoury, R., 2004. Earthquake Hazard in Lebanon. Imperial College Press, London.

Salamon, A., Rockwell, T., Guidoboni, E., Comastri, A., 2010. A critical evaluation of tsunami records reported for the Levant coast from the second millennium BCE to the present, Israel. Israel Journal of Earth Sciences, **58:** 327–354; https://doi.org/10.1560/IJES.58.2-3.327

Salamon, A., Omira, R., Zohar, M., Baptista, M.A., 2024. Modern outlook on the source of the 551 AD tsunamigenic earthquake that struck the Phoenician (Lebanon) coast. Natural Hazards, **120:** 8893–8929; https://doi.org/10.1007/s11069-024-06559-4

Sanlaville, P., 1977. Etude géomorphologique de la région littorale du Liban (in Polish). Ph.D. thesis, Lebanese University, Beirut.

Sánchez-Sánchez, Y., Elez, J., Silva, P.G., Santos-Delgado, G., Giner-Robles, J.L., Reicherter, K., 2022. 3D modelling of archaeoseismic damage in the Roman site of *Baelo Claudia* (Gibraltar Arc, South Spain), Applied Sciences3D modelling of archaeoseismic damage in the Roman site of Baelo Claudia (Gibraltar Arc, South Spain). Applied Sciences, **12**, 5223; https://doi.org/10.3390/app12105223

Sbeinati, M.R., Darawcheh, R., Mouty, M., 2005. The historical earthquakes of Syria: an analysis of large and moderate earthquakes from 1365 B.C. to 1900 A.D. Annals of Geophysics-Italy, **48:** 347–435.

Scheffers, A., Kelletat, D., 2003. Sedimentologic and geomorphologic tsunami imprints worldwide – a review. Earth-Science Reviews, **63:** 83–92; https://doi.org/10.1016/S0012-8252(03)00018-7

Scholz, C., 1982. Scaling laws for large earthquakes: consequences for physicalmodels. Bulletin of the Seismological Society of America, **72:** 1–14; https://doi.org/10.1785/BSSA0720010001

Shanmugam, G., 2006. The tsunamite problem. Journal of Sedimentary Research, **76:** 718–730; https://doi.org/10.2110/jsr.2006.073

Shanmugam, G., 2012. Process-sedimentological challenges in distinguishing paleo-tsunami deposits. Natural Hazards, **63:** 5–30; https://doi.org/10.1007/s11069-011-9766-z

Shiki, T., Tsuji, Y., Yamazaki, T., Nanayama, F., 2021. Tsunamities. Features and Implications, Elsevier.

Sieberg, A., 1932. Untersuchungen über Erdbeben und Bruchschollenban im östlichen Mittelmeergebiet. Denkschriften der Medizinish-Naturwissenschaftlichen Gesellschaft zu Jena, **18:** 161-273.

Skiple, C., Anderson, E., Fürstenau, J., 2012. Seismic interpretation and attribute analysis of the Herodotus and the Levantine Basin, offshore Cyprus and Lebanon. Petroleum Geosciences, **18:** 433–442; https://doi.org/10.1144/petgeo2011-072

Soloviev, S.L., Solovieva, O.N., Go, C.N., Kim, C.S., Shchetnikov, N.A., 2000. Tsunamis in the Mediterranean Sea 2000 B.C.–2000 A.D. Advances in Natural and Technological Hazards Research. Kluwer, Dordrecht.

Soysal, H., 1985. Tsunami (Deniz taṭması) ve Türkiye kıyılarını etkileyen tsunamiler (in Turkish). Deniz Bilimleri ve Coğrafya Enstitüsü Bülteni, **2:** 59–67.

Soysal, H., Sipahiođlu, S., Kolçak, D., Altýnok, Y., 1981. Türkiye ve Çevresinin Tarihsel Deprem Katalogu (MÖ 2100-MS1900) (in Turkish). TÜBİTAK.

Staniszewski, R., Filipek, A., Wysocka, A., 2025. The propagation of tsunami waves over time (selected faults from Eastern Mediterranean Coast) [dataset], Institute of Geological Sciences Polish Academy of Sciences, v2; https://doi.org/10.60871/INGPAN/REQEON

Stiros, S.C., 2001. The AD 365 Crete earthquake and possible seismic clustering during the fourth to sixth centuries in the Eastern Mediterranean: a review of historical and archaeological data. Journal of Structural Geology, **23:** 545–562; https://doi.org/10.1016/S0191-8141(00)00118-8

Sugawara, D., 2021. Numerical modelling of tsunami: advances and future challenges after the 2011 Tohoku earthquake and tsunami. Earth-Science Reviews, **214**, 103498; https://doi.org/10.1016/j.earscirev.2020.103498

Tadibaght, A., El M'rini, A., Siame, L., Bellier, O., 2022. Tsunami impact assessment for low-lying cities along the Northern Atlantic coast of Morocco using MIRONE software. Journal of African Earth Sciences, **192,** 104580; https://doi.org/10.1016/j.jafrearsci.2022.104580

Trombley, F.R., 2000. The Chronicle of Pseudo-Joshua the Stylite. University Press, Liverpool.

Vött, A., Bruins, H.J., Gawehn, M., Goodman-Tchernov, B.N., De Martini, P.M., Kelletat, D., Mastronuzzi, G., Reicherter, K., Röbke, B.R., Scheffers, A., Willershäuset, T., Avramidis, P., Bellanova, P., Costa, P.J.M., Finkler, C., Hadler, H., Koster, B., Lario, J., Reinhardt, E., Ntageretzis, K., Pantosti, D., Mathes-Schmidt, M., Papanikolaou, I Sansò, P., Scicchitano, G., Smedile, A., Szczuciński, W., 2019. Publicity waves based on manipulated geoscientific data suggesting climatic trigger for majority of tsunami findings in the Mediterranean, response to 'Tsunamis in the geological record: making waves with a cautionary tale from the Mediterranean' by Marriner et al., 2017. Zeitschrift für Geomorphologie, **62:** 7–45; https://doi.org/10.1127/zfg_suppl/2018/0547

Waliszewski, T., Gwiazda, M., 2015. Porphyreon through the ages. The Fading Archaeological Heritage of the Lebanese Coast. Journal of Eastern Mediterranean Archaeology & Heritage Studies, **3:** 330–348; https://doi.org/10.5325/jeasmedarcherstu.3.4.0330

Wang, J., Ye, Z.-R., He, J.-K., 2008. Three-dimensional mechanical modelling of large-scale crustal deformation in China constrained by the GPS velocity field. Tectonophysics, **446:** 51–60; https://doi.org/10.1016/j.tecto.2007.11.006

Ward, W.D., 2016. The 363 Earthquake and the End of Public Paganism in the Southern Transjordan. Journal of Late Antiquity, **9:** 132–170; https://doi.org/10.1353/jla.2016.0003

Wicenciak, U., 2016. Porphyreon. Hellenistic and Roman Pottery Production in the Sidon Hinterland, The Polish Centre of Mediterranean Archaeology PAM Monograph Series 7. University of Warsaw Press, Warsaw.

Wicenciak, U., El-Tayeb, M., 2006. Section C – Jiyeh, 2005 season. Bulletin d'Archeologie et d'Architecture Libanaises, **10** (5–85): 67–79.

Williams, A.T., Caldwell, N.E., 1988. Particle size and shape in pebble-beach sedimentation. Marine Geology, **82:** 199–215; https://doi.org/10.1016/0025-3227(88)90141-7

Witakowski, W., 1996. Pseudo-Dionysius of Tel-Mahre: Chronicle, Part III. Liverpool University Press, Liverpool.

Yolsal, S., Taymaz, T., Yalçiner, A.C., 2007. Understanding tsunamis, potential source regions and tsunami prone mechanisms in the Eastern Mediterranean. Geological Society Special Publications, **291:** 201–230; https://doi.org/10.1144/SP291.10

Yu, N.-T., Yen, J.-Y., Yen, I.-Ch., Hirakawa, K., Chuang, C.-M., 2020. Tsunami deposits and recurrence on a typhoon-prone coast of northern Taiwan from the last millennium. Quaternary Science Reviews, **245**, 106488; https://doi.org/10.1016/j.quascirev.2020.106488

Zhang, X., Sanderson, D.J., 1996. Numerical modelling of the effects of fault slip on fluid flow around extensional faults. Journal of Structural Geology, **18:** 109–119; https://doi.org/10.1016/0191-8141(95)00086-S

Zumoffen, P.G., 1926. Carte Géologique du Liban. Henry Barrère, Éditeur – Géographe. Paris.

APPENDIX 1

Summary of fault parameters used for modelling

Fault	Mag	Length [km]	Width [km]	Strike [degrees]	Dip [degrees]	Depth [km]	Depht to top [km]	Rake [degrees]	Slip [m]	Shear modulus [10^10]	note	max slip [m]	slip confirmation
1	8	55,6422	13,9105	125	80	39,6992	26	10	22	6,80		12	0
1	7,0	55,64	13,91	125	80,0	39,7	26	10,0	0,8	6,8		12	1
1	7,5	55,64	13,91	125	80,0	39,7	26	10,0	4,0	6,8		12	1
2	7,0	60,23	15,06	288,8	35,0	32,6	24,0	100,0	0,7	6,8		12	1
2	7,5	60,23	15,06	288,8	35,0	32,6	24,0	100,0	3,1	6,8		12	1
2	8,0	60,23	15,06	288,8	35,0	32,6	24,0	100,0	18,0	6,8		12	0
3	8	45,3149	11,1952	284,9	30	30,5976	25	90	34	6,80		12	0
3	7,0	45,31	11,20	284,9	30,0	30,6	25,0	90	1,0	6,8		12	1
3	7,5	45,31	11,20	284,9	30,0	30,6	25,0	90,0	5,5	6,8		12	1
4	7,0	56,16	14,04	286,5	25	26,9	21,0	90,0	0,8	6,8		12	1
4	8	56,1569	14,0392	286,5	25	26,9332	21	90	25	6,80		12	0
4	7,5	56,16	14,04	286,5	25	26,9	21	90	4,5	6,8		12	1
5	8	46,5938	11,6485	87,5	25	18,9229	14	63	46	4,4		12	0
5	7,0	46,59	11,65	87,5	25	18,9	14	63	1,5	4,4		12	1
5	7,5	46,59	11,65	87,5	25	18,9	14	63	11,0	4,4		12	1
6	8	42,3557	10,5889	80,7	25	31,4751	27	80	35	6,80		12	0
6	7,0	42,36	10,59	80,7	25,0	31,5	27	80	1,4	6,8		12	1
6	7,5	42,36	10,59	80,7	25,0	31,5	27	80	7,0	6,8		12	1
7	7,5	54,68	14,47	291,5	70	33,6	20	170	0,8	6,8		12	1
7	7	54,681	14,4694	291,5	70	33,5968	20	170	?	6,80		12	0
7	8,0	54,68	14,47	291,5	70	33,6	20	170	4,0	6,8		12	1
8	7,0	74,65	18,66	44	80	34,4	16	30	0,4	6,8		14	1
8	7,5	74,65	18,66	44	80	34,4	16	30	2,8	6,8		14	1
8	8,0	74,65	18,66	44	80	34,4	16	30	14,0	6,8		14	1
9	8	51,6923	12,9231	295,4	25	14,4615	9	125	65	2,60		12	0
9	7,0	51,69	12,92	295,4	25	14,5	9	125	2,5	2,6		12	1
9	7,5	51,69	12,92	295,4	25	14,5	9	125	11,0	2,6		12	1
10	7,5	32,3544	8,0886	304,3	35	32,6394	28	120	11	6,80		10	0
10	8	32,3544	8,0886	304,3	35	32,6394	28	120	61	6,80		10	0
10	7,0	32,35	8,09	304,3	35	32,6	28	120	1,9	6,8		10	1
11	7,0	56,92	14,23	98,6	20	20,9	16	70	1,0	4,4		12	1
11	8	56,9171	14,2293	98,6	20	20,8667	16	70	30	4,40		12	0
11	7,5	56,92	14,23	98,6	20	20,9	16	70	6,0	4,4		12	1
12	7,5	34,3298	8,5824	274,9	30	24,2912	20	80	15	4,40		10	0
12	8	34,3298	8,5824	274,9	30	24,2912	20	80	82	4,40		10	0
12	7,0	34,33	8,58	274,9	30	24,3	20	80	2,6	4,4		10	1
13	7,5	30,3629	7,5907	270,1	25	25,208	22	85	13	6,80		10	0
13	8	30,3629	7,5907	270,1	25	25,208	22	85	68	6,80		10	0
13	7,0	30,36	7,59	270,1	25,0	25,2	22	85	2,8	6,8		10	1
14	7,5	31,1252	7,7813	232,1	70	35,312	28	-20	12	6,80		10	0
14	8	31,1252	7,7813	232,1	70	35,312	28	-20	68	6,80		10	0
14	7,0	31,13	7,78	232,1	70	35,3	28	-20	2,6	6,8		10	1
15	7,5	29,5104	7,3776	331	75	32,1262	25	160	13	6,80		7	0
15	8	29,5104	7,3776	331	75	32,1262	25	160	72	6,80		7	0
15	7,0	29,51	7,38	331,0	75	32,1	25	160	2,8	6,8		7	1
16	8	22,1449	5,5362	326,9	75	30,3476	25	145	130	6,80		7	0
16	7,5	22,1449	5,5362	326,9	75	30,3476	25	145	24	6,80		7	0
16	7,0	22,14	5,54	326,9	75	16,0	25	145	6,5	4,4		7	1
17	7,0	(17a, 17b)	(17a, 17b)	(17a, 17b)	(17a, 17b)	(17a, 17b)	(17a, 17b)	(17a, 17b)	0,1	6,8		(17a, 17b)	1
17	7,5	(17a, 17b)	(17a, 17b)	(17a, 17b)	(17a, 17b)	(17a, 17b)	(17a, 17b)	(17a, 17b)	0,8	6,8		(17a, 17b)	1
17	8,0	(17a, 17b)	(17a, 17b)	(17a, 17b)	(17a, 17b)	(17a, 17b)	(17a, 17b)	(17a, 17b)	4,0	6,8		(17a, 17b)	1
18	7,0	(18a, 18b, 18c,)	(18a, 18b, 18c,)	(18a, 18b, 18c,)	(18a, 18b, 18c,)	(18a, 18b, 18c,)	(18a, 18b, 18c,)	(18a, 18b, 18c,)	0,2	6,8		(18a, 18b, 18c.	1
18	7,5	(18a, 18b, 18c,)	(18a, 18b, 18c,)	(18a, 18b, 18c,)	(18a, 18b, 18c,)	(18a, 18b, 18c,)	(18a, 18b, 18c,)	(18a, 18b, 18c,)	1,2	6,8		(18a, 18b, 18c.	1
18	8,0	(18a, 18b, 18c,)	(18a, 18b, 18c,)	(18a, 18b, 18c,)	(18a, 18b, 18c,)	(18a, 18b, 18c,)	(18a, 18b, 18c,)	(18a, 18b, 18c,)	6,5	6,8		(18a, 18b, 18c.	1
19	7,0	57,33	14,33	154,4	45	24,1	14	-160	1,3	4,4		12	1
19	8	57,3292	14,3323	154,4	45	24,1345	14	-160	30	4,40		12	0
19	7,5	57,33	14,33	154,4	45	24,1	14	-160	6,0	4,4		12	1
20	8	24,902	6,2255	33,6	25	22,63101	20	110	158	4,40		7	0
20	7,5	24,902	6,2255	33,6	25	22,63101	20	110	28	4,40		7	0
20	7,0	24,90	6,23	33,6	25,0	22,6	20	110,0	5,0	4,4		7	1
21	8	22,7771	5,6943	39,4	30	20,8471	18	130	188	4,40		7	0
21	7,5	22,7771	5,6943	39,4	30	20,8471	18	130	36	4,40		7	0
21	7,0	22,78	5,69	39,4	30	20,8	18	130	6,0	4,4		7	1
22	8	11,4714	2,8678	42,6	25	21,212	20	70	-	x		4	0
22	7,5	11,4714	2,8678	42,6	25	21,212	20	70	138	4,40		4	0
22	7	11,4714	2,8678	42,6	25	21,212	20	70	27	4,40		4	0
23	8	11,5155	2,8789	50,8	25	21,2167	20	80	-	x		4	0
23	7,5	11,5155	2,8789	50,8	25	21,2167	20	80	130	4,4		4	0
23	7	11,5155	2,8789	50,8	25	21,2167	20	80	26	4,4		4	0
24	7,5	10,7971	2,6993	55,8	25	21,1408	20	80	148	4,4		4	0
24	7	10,7971	2,6993	55,8	25	21,1408	20	80	28	4,4		4	0
25	7,0	47,83	11,96	263,8	80	31,8	20	165	1,2	6,8		12	1

25	8	47,8304	11,9576	263,8	80	31,7759	20	165	28	6,8		12	0
25	7,5	47,83	11,96	263,8	80	31,8	20	165	6,5	6,8		12	1
26	8	20,008	5,002	262,5	80	26,926	22	170	170	6,8		7	0
26	7,5	20,008	5,002	262,5	80	26,926	22	170	28	6,8		7	0
26	7,0	20,01	5,00	262,5	80	26,9	22	170	5,0	6,8		7	1
27	8	13,3549	3,3387	28,9	25	11,411	10	100	-	x		4	0
27	7,5	13,3549	3,3387	28,9	25	11,411	10	100	164	2,6		4	0
27	7	13,3549	3,3387	28,9	25	11,411	10	100	30	2,6		4	0
28	7,5	6,50102	1,6253	16,2	25	16,6869	16	80	-	4,40		1	0
28	8	6,50102	1,6253	16,2	25	16,6869	16	80	-	4,40		1	0
28	7	6,50102	1,6253	16,2	25	16,6869	16	80	80	4,40		1	0
29	7	9,46083	2,3652	26,5	25	10,9996	10	90	58	2,60		1	0
30	7,0	(30a, 30b, 30c)	(30a, 30b, 30c)	(30a, 30b, 30c)	(30a, 30b, 30c)	(30a, 30b, 30c)	(30a, 30b, 30c)	(30a, 30b, 30c)	2,6	(30a, 30b, 30c)		12	1
30	8	(30a, 30b, 30c)	(30a, 30b, 30c)	(30a, 30b, 30c)	(30a, 30b, 30c)	(30a, 30b, 30c)	(30a, 30b, 30c)	(30a, 30b, 30c)	70	(30a, 30b, 30c)		12	0
30	7,5	(30a, 30b, 30c)	(30a, 30b, 30c)	(30a, 30b, 30c)	(30a, 30b, 30c)	(30a, 30b, 30c)	(30a, 30b, 30c)	(30a, 30b, 30c)	12,0	(30a, 30b, 30c)		12	1
31	7,0	(31a, 31b, 31c, 31d)	(31a, 31b, 31c, 31d)	(31a, 31b, 31c, 31d)	(31a, 31b, 31c, 31d)	x	(31a, 31b, 31c, 31d)	(31a, 31b, 31c, 31d)	2,0	(31a, 31b, 31c, 31d)		12	1
31	7,5	(31a, 31b, 31c, 31d)	(31a, 31b, 31c, 31d)	(31a, 31b, 31c, 31d)	(31a, 31b, 31c, 31d)	x	(31a, 31b, 31c, 31d)	(31a, 31b, 31c, 31d)	11,0	(31a, 31b, 31c, 31d)		12	1
31	8,0	(31a, 31b, 31c, 31d)	(31a, 31b, 31c, 31d)	(31a, 31b, 31c, 31d)	(31a, 31b, 31c, 31d)	x	(31a, 31b, 31c, 31d)	(31a, 31b, 31c, 31d)	59,0	(31a, 31b, 31c, 31d)		12	0
32	8	13,201	3,3002	189,8	25	19,3947	18	90	-	4,4		4	0
32	7	13,201	3,3002	189,8	25	19,3947	18	90	18	4,4		4	0
32	7,5	13,201	3,3002	189,8	25	19,3947	18	90	99	4,4		4	0
33	7,0	28,47	7,12	36,7	25,0	28,0	25	90	2,5	6,8		7	1
33	7,5	28,47	7,1175	36,7	25	28,008	25	90	14	6,8		7	0
33	8	28,47	7,1175	36,7	25	28,008	25	90	78	6,8		7	0
34	7,0	29,78	7,45	88,1	60	21,4	15	-170	3,5	4,4		7	1
34	8	29,7824	7,4456	88,1	60	21,4481	15	-170	115	4,4		7	0
34	7,5	29,7824	7,4456	88,1	60	21,4481	15	-170	20	4,4		7	0
35	7,0	39,60	9,90	68,6	60	28,6	20	-165	1,3	6,8		10	1
35	8	39,596	9,899	68,6	60	28,5728	20	-165	40	6,8		10	0
35	7,5	39,60	9,90	68,6	60	28,6	20	-165	7,1	6,8		10	1
36	7	12,5655	3,1414	8,7	25	9,32761	8	90	40	2,60		4	0
37	7	13,4302	3,3576	258,7	70	13,1551	10	165	29	2,60	no deformations	4	0
38	7	12,2695	3,0674	56,8	25	16,2963	15	90	21	4,40		4	0
39	7,5	23,3355	5,8339	54,8	25	17,4655	15	90	32	4,4		7	0
39	7,0	23,34	5,83	54,8	25,0	17,5	15	90	6,0	4,4		7	1
40	7	15,3025	3,8256	34	25	16,6168	15	90	14	4,40		4	0
40	7,5	15,3025	3,8256	34	25	16,6168	15	90	75	4,40		4	0
41	7,0	32,04	8,01	79,1	35	4,6	0	50	5,2	2,6		10	1
41	8	32,0414	8,0104	79,1	35	4,59458	0	50	160	2,6		10	0
41	7,5	32,0414	8,0104	79,1	35	4,59458	0	50	29	2,6		10	0
42	7,0	27,96	6,99	250,7	80	26,9	20	170	2,8	6,8		7	1
42	7,5	27,9646	6,9911	250,7	80	26,8849	20	170	14,5	6,8		7	0
42	8	27,9646	6,9911	250,7	80	26,8849	20	170	80	6,8		7	0
17a	7,0	84,14	21,03	236,3	25	28,9	20	30,0	0,3	6,8		14	1
17a	7,5	84,14	21,03	236,3	25	28,9	31	30,0	1,8	6,8		14	1
17a	8,0	84,14	21,03	236,3	25	28,9	31	30,0	9,0	6,8		14	1
17b	7,0	106,65	26,66	258,4	25,0	36,3	25	70,0	0,2	6,8		14	1
17b	7,5	106,65	26,66	258,4	25,0	36,3	25	70,0	1,0	6,8		14	1
17b	8,0	106,65	26,66	258,4	25,0	36,3	25	70,0	9,0	6,8		14	1
18a	7,0	52,06	13,00	208,2	43	28,9	20	-10	1,0	6,8		12	1
18a	7,5	52,06	13,00	208,2	43	28,9	20	-10	5,0	6,8		12	1
18a	8	52,0618	13	208,2	43	28,866	20	-10	25	6,80		12	0
18b	7,0	65,56	13,00	237,4	30	31,5	25	20	0,8	6,8		12	1
18b	7,5	65,56	13,00	237,4	30	31,5	25	20	4,0	6,8		12	1
18b	8	65,5637	13	237,4	30	31,5	25	20	19	6,80		12	0
18c	7,0	55,07	13,00	261,1	27	30,9	25	70	0,9	6,8		12	1
18c	7,5	55,07	13,00	261,1	27	30,9	25	70	5,0	6,8		12	1
18c	8	55,0711	13	261,1	27	30,9019	25	70	22	6,80		12	0
18d	7,0	243,50	13,00	243,5	25	30,5	25	90	1,1	6,8		16	1
18d	7,5	243,50	13,00	243,5	25	30,5	25	90	6,0	6,8		16	1
18d	8	243,5	13	243,5	25	30,494	25	90	29	6,80		16	0
30a	-	18,178	8	26,6	25	21,3809	18	90	-	6,80		-	0
30b	-	17,6982	10	356,9	25	22,2262	18	90	-	6,80		-	0
30c	-	6,0435	8	18,4	25	21,3809	18	90	-	6,80		-	0
31a	-	18,4301	8	352,2	25	17,3809	14	90	-	4,4		-	0
31b	-	11,9994	10	23,4	25	18,2262	14	90	-	4,4		-	0
31c	-	9,13854	10	52,8	25	18,2262	14	90	-	4,4		-	0
31d	-	7,02091	8	4,1	25	17,3809	14	90	-	4,4		-	0